FREE-FLIGHT INVESTIGATION OF THE AERODYNAMIC CHARACTERISTICS OF A 10-DEG SEMIANGLE CONE AT MACH NUMBERS FROM 6 TO 16

C. J. Welsh, G. L. Winchenbach, and A. N. Madagan

ARO, Inc.

April 1969

VON KÁRMÁN GAS DYNAMICS FACILITY
ARNOLD ENGINEERING DEVELOPMENT CENTER
AIR FORCE SYSTEMS COMMAND
ARNOLD AIR FORCE STATION, TENNESSEE

NOTICES

FREE-FLIGHT INVESTIGATION OF THE AERODYNAMIC CHARACTERISTICS OF A 10-DEG SEMIANGLE CONE AT MACH NUMBERS FROM 6 TO 16

C. J. Welsh, G. L. Winchenbach, and A. N. Madagan

ARO, Inc.

FOREWORD

This technical report has been reviewed and is approved.

David C. Reynolds
1st Lt, USAF
Research Division
Directorate of Plans
   and Technology

Edward R. Feicht
Colonel, USAF
Director of Plans
   and Technonogy

ABSTRACT

A 1000-ft hypervelocity range was used to obtain the free-flight static and dynamic stability and drag data presented for a 10-deg semi-angle cone. Measurements indicate that the damping-in-pitch derivatives for the cone increase appreciably with increasing Mach number between M = 8 and 16 at a Reynolds number (based on model length and free-stream conditions) of about 0.4 x 10^6. Further, $C_{m\alpha}$ for the cone decreases significantly as the nose-radius to base-radius ratio of the cone is increased up to 0.1 for amplitudes greater than about 5 deg. Comparisons of the range stability data with wind tunnel data (involving sting-supported models) obtained in different test facilities indicate that appreciable differences in $C_{m\alpha}$ and ($C_{mq} + C_{m\dot{\alpha}}$) exist in some cases.

TRANSMITTAL NOTE

1. The attached report is forwarded for your information
    and retention.

2. Inquiries relative to any feature of this report should
    be addressed to this Headquarters, ATTN: AETS.

ROY R. CROY, JR., Colonel, USAF
Director of Test

CONTENTS

APPENDIX

Illustrations

Figure   Page

NOMENCLATURE

C_D	Drag coefficient
C_{D_o}	Drag coefficient at zero angle of attack
$C_{L\alpha}$	Lift-force derivative
$C_{mq} + C_{m\dot\alpha}$	Damping-in-pitch derivatives,

$$\frac{\partial C_m}{\partial q(d/2V)} + \frac{\partial C_m}{\partial \dot\alpha (d/2V)}$$

$C_{m\alpha}$	Pitching-moment derivative
$C_{Np\alpha}$	Magnus-force derivative
$C_{N\alpha}$	Normal-force derivative
C_p	Pressure coefficient
C_{yo}	Side-force coefficient at $\xi = 0$
C_{zo}	Normal-force coefficient at $\xi = 0$
cg	Position of the center of gravity, percentage of model length from the nose
cp	Position of the center of pressure, percentage of model length from the nose

D	Damping parameter (see Eq. (6))
d	Model diameter, and moment reference length
I_x	Model moment of inertia (relative to a longitudinal axis)
I_y	Model moment of inertia (relative to a transverse axis)
K_1, K_2, K_3	Constants in Eq. (4)
k_o	Slope of C_D versus $\overline{\delta^2}$ curve
L_1, L_2	Integration limits in Eq. (2)
ℓ	Model length
M	Mach number
m	Model mass
p	Model roll rate referenced to distance traveled
R_B	Base radius of model
Re_ℓ	Reynolds number based on free-stream conditions and model length
R_N	Nose radius of model
S	Reference area based on model base diameter
V	Model velocity
X_{cg}	Distance to center of gravity from the model nose
X_{cp}	Distance to center of pressure from the model nose
x	Distance along flight path
$y + iz$	Transverse displacement of model center of gravity
α_{mean}	Mean angle of attack
α_o	Initial angle of attack
β, α	Components of the complex yaw angle
δ_1	Local body slope with respect to the free-stream velocity
$\overline{\delta}$	$\sqrt{\left(\frac{1}{L_2 - L_1}\right) \int_{L_1}^{L_2} \overline{(\beta^2 + \alpha^2)}\, dx}$
δ^2	$\alpha^2 + \beta^2$
θ_c	Cone semiangle
μ_1, μ_2	Damping rates of vectors in Eq. (4)

ξ	Complex yaw angle, $\beta + i\alpha$
ρ	Mass density of the range air
σ_y	Radius of gyration (relative to a transverse axis)
ϕ_1', ϕ_2'	Rates of rotation of vectors in Eq. (4)
ω	Angular frequency

SUPERSCRIPTS

$'$	First derivative with respect to distance
$''$	Second derivative with respect to distance

SECTION I
INTRODUCTION

Aerodynamic characteristics of slender cones have received a considerable amount of attention from various investigators in recent years; however, only a very limited amount of experimental stability data for cones at high Mach numbers has been published. Concern has existed regarding some of these stability measurements made in the past because of apparent inconsistencies in the test results (see, for example, the comments of Hobbs in Ref. 1). Concern has also existed regarding an apparent stability problem detected in previous cone testing, specifically, damping derivatives decreasing to near zero with increasing Mach numbers, as has been observed in wind tunnel tests of a 10-deg semiangle cone at Mach numbers between 10 and 20.

In consideration of the factors noted in the above comments, it was felt that some free-flight stability measurements for cones could be of particular significance. Hence, a series of free-flight tests has been made in which the aerodynamic characteristics of a 10-deg semiangle cone have been investigated at Mach numbers from 6 to 16 for Reynolds numbers, based on model lengths and free-stream conditions, from 0.2×10^6 to 11×10^6. The tests were conducted in the von Kármán Gas Dynamics Facility (VKF), Arnold Engineering Development Center (AEDC) 1000-ft Hypervelocity Range G.

The purpose of this report is to present the results of this investigation, including both stability and drag data. Further, the range stability derivatives are compared with analytically predicted values and with wind tunnel data obtained in different facilities.

SECTION II
APPARATUS

2.1 RANGE

The VKF Range G consists of a 10-ft-diam, 1000-ft-long tank contained within an underground tunnel (see Fig. 1). It is a variable density aerodynamic range and has an 840-ft instrumented length that includes 43 equally spaced, dual-plane shadowgraph stations. The shadowgraph system permits determining the angular orientation and position of most test configurations to within approximately ±0.25 deg and ±0.002 ft, respectively, at each station. A chronograph system measures intervals

of flight time to within $\pm 2 \times 10^{-7}$ sec. The range vacuum pumping system provides range pressures from one atmosphere down to about 15 μHg. The 15-μHg pressure level corresponds to an equivalent altitude of approximately 250,000 ft. The nominal operating temperature of the range is 76°F. The launcher normally used with the range is a two-stage, light-gas gun having a 2.5-in.-diam launch tube.

2.2 MODELS AND SABOTS

The configuration investigated was a 10-deg semiangle cone, and the models used had a nominal base diameter of either 1 or 1.75 in. and a designed nose-to-base-radius ratio (R_N/R_B) of either 0.035 or 0.07. The models were constructed basically of either aluminum or steel; however, models designed for testing at the higher heating conditions were equipped with copper nose tips.

The sabots used in the test program were of a conventional four-component design and were aerodynamically separated from the models in the blast tank portion of the range. All models were launched in an uncanted orientation relative to the sabot, and the initial angular disturbances to the models were those arising from muzzle effects and from the model-sabot separation process.

SECTION III
DATA REDUCTION

3.1 GENERAL COMMENTS

The basic data reduction procedures associated with aeroballistic range testing are discussed in various reports, for example Refs. 2 through 4. A discussion of the effects of small roll rates on the yawing motion of statically stable bodies and the limitations associated with certain simplified data analysis procedures can be found in Ref. 5. In the present test program, the aerodynamic data were reduced from the measured position-attitude-time histories of the free-flight models using basic range techniques which involved the following computer programs.

3.2 DRAG PROGRAM

The drag coefficient, C_D, is obtained from the relation

$$C_D = - (2m/\rho S \overline{V}) (dV/dx) \tag{1}$$

where dV/dx is the mean slope of the curve of model velocity as a function of distance traveled, and $\bar{V}$ is the mean model velocity during the interval of the flight trajectory being examined. The velocity data used are the average velocities between consecutive stations as obtained from the measured position-time history of the model. The term dV/dx is obtained by fitting a linear equation to the velocity-distance data by means of a least squares procedure. Equation (1) is based on the assumption that C_D is constant during the flight interval of concern and has been found to provide quite adequate results when the total velocity drop during the flight interval is less than about five percent of the initial velocity. Since the angle of attack of a model, in general, will vary along the trajectory, the drag coefficient obtained by this procedure corresponds to the mean total angle of attack experienced by the model. This mean angle of attack is defined by the relation

$$\overline{\delta^2} = [1/(L_2 - L_1)] \int_{L_1}^{L_2} \delta^2 \, dx \tag{2}$$

where $L_2 - L_1$ is the length of the flight interval over which C_D is computed.

The mean drag coefficient obtained from Eq. (1) can be adjusted to zero yaw angle with use of the relationship

$$C_D = C_{D_0} + k_0 \overline{\delta^2} \tag{3}$$

In the present tests, values used for k_0 were obtained from the plot of k_0 as a function of Mach number shown in Fig. 2. The k_0 variation of Fig. 2 was obtained by fairing a curve through k_0 values determined at four different nominal Mach numbers. The k_0 value at each nominal Mach number was evaluated from plots of different shots near that Mach number but having different values of $\overline{\delta^2}$. No appreciable effect of Reynolds number on k_0 was detected in the present data.

3.3 YAW PROGRAM

The static-stability derivative and the total damping parameter were evaluated in an analysis of the angular motion of the model with the following equation:

$$\xi = K_1 \exp\left[(\mu_1 + i\phi_1')x\right] + K_2 \exp\left[(\mu_2 + i\phi_2')x\right] + K_3 \exp(ipx) \tag{4}$$

Equation (4), defining tricyclic motion, is the solution of the linear differential equation (Ref. 4) for general rolling, yawing model motion. The equation corresponds to a right-hand, nonrolling body axis system,

3

and its use is restricted to models having only slight configurational asymmetries, near linear variations of force and moment with yaw angle, and small changes in p. Equation (4) is fitted to the measured components of the complex yaw angle as functions of distance traveled, using a differential corrections procedure. There are ten equation constants to be determined in fitting Eq. (4). The K's, in general, are complex numbers; however, p can be expressed as a function of ϕ_1' and ϕ_2'. The desired stability parameters can be expressed in terms of the determined equation constants by the following relationships:

$$C_{m\alpha} = (2I_y/d\rho S)\ \phi_1'\ \phi_2' \tag{5}$$

$$D = -C_{L\alpha} - C_D + (1/2)\ (d/\sigma_y)^2\ (C_{mq} + C_{m\dot{\alpha}}) = (\mu_1 - \mu_2)\ (2m/\rho S) \tag{6}$$

In fitting an equation using the differential corrections procedure, which is an iterative process, it is necessary to determine first a set of approximate or initial values for the equation constants to be evaluated. The errors in the initial values must be sufficiently small to permit the iterative process to converge. For aerodynamically stable models, the initial values for the constants can be determined analytically using a procedure based on the Prony Method discussed in Ref. 6. Input data for computing the initial values are the measured β and α, and distance values corresponding to six or more shadowgraph stations of near equal spacing. In general, the angular motion of the models of the present tests was of a precessing elliptical nature (complex yaw angle plane), and the analytically determined initial values were quite adequate.

3.4 SWERVE PROGRAM

The lift-curve slope is obtained from an analysis of the transverse motion of the model (Ref. 4). The differential equation defining the transverse motion, referenced to a right-hand, range-fixed coordinate system with the x-axis along the range axis, can be written as

$$y'' + iz'' = -(\rho S/2m)\ [(C_{L\alpha} + ipd\ C_{Np\alpha})\ \xi - (C_{yo} + iC_{zo})\ \exp\ (ipx)] \tag{7}$$

This equation may be integrated to yield

$$y + iz = (y_0 + iz_0) + (y_0' + iz_0')x - (C_{L\alpha} + ipd\ C_{Np\alpha})\ (G + iH) + \tag{8}$$

$$(C_{yo} + iC_{zo})\ (I + iJ)$$

where

$$G + iH = (\rho S/2m) \int_0^{x_1} \int_0^{x_2} \xi\ dx_1\ dx_2$$

$$I + iJ = (\rho S/2mp^2)[(1 - \cos px) + i(px - \sin px)]$$

and zero subscripts indicate initial values. Equation (8) is fitted to the measured $(y + iz)$ values by a least-squares curve-fitting procedure to obtain $C_{L\alpha}$. For the small roll rates involved in the present tests, the $C_{Np\alpha}$ term was negligibly small.

The normal-force derivative is obtained from the relation

$$C_{N\alpha} = C_{L\alpha} + C_D \tag{9}$$

and the center of pressure is computed as

$$X_{cp}/\ell = (X_{cg}/\ell) - (C_{m\alpha}/C_{N\alpha})(d/\ell) \tag{10}$$

With both $C_{L\alpha}$ and C_D evaluated, the damping-in-pitch derivatives, $C_{mq} + C_{m\dot{\alpha}}$, were obtained from the total damping parameter, D (see Eq. (6)). It should be noted that stability derivatives reduced using the linear analysis discussed above are "effective" derivatives, if the model involved has force and moment variations that are slightly nonlinear.

3.5 PRECISION OF MEASUREMENTS

The estimated maximum probable errors in the data presented in this report are listed below:

	C_{D_o}	$C_{m\alpha}$	$(C_{mq} + C_{m\dot{\alpha}})$	$C_{N\alpha}$	cp
Probable Error, %	±4	±3	±10	±5	±0.3

SECTION IV
BALLISTIC RANGE TESTS

4.1 DYNAMIC STABILITY DERIVATIVES

Measured $C_{mq} + C_{m\dot{\alpha}}$ values as a function of Reynolds number, for Mach numbers near 6.5, are shown in Fig. 3. The level and trend of the damping values for a laminar boundary layer ($Re_\ell < 4.5 \times 10^6$) are well defined. For the higher Reynolds number shots ($Re_\ell > 4.5 \times 10^6$) the location of transition is in the region of the model base. The increased spread in the measurements at the highest Reynolds numbers is believed to be related to fluctuations in the location of transition and is indicative of the increased difficulty in obtaining consistent damping measurements for this test condition. The damping levels predicted by the shock expansion method (Ref. 7) and the unsteady flow field method

(Ref. 8) are also shown in Fig. 3, and both are lower than that indicated by the range data.

Damping derivatives as a function of Mach number, for $Re_\ell \approx$ 0.4 x 10^6, are presented in Fig. 4. Except for the two low data points (square symbols) at M ≈ 15, the measurements are quite consistent and indicate a marked increase in damping with increasing Mach number. The circular symbols represent shots for which the models experienced nonplanar motion patterns, but these patterns were comparable to model motion in one-degree-of-freedom wind tunnel tests; that is, the model on these shots experienced a near zero transverse velocity component (component normal to the angle-of-attack plane) at its maximum amplitude. The other three shots (square symbols) had combinations of a rolling velocity and a wider elliptic motion pattern such that the model would tend to have a larger transverse velocity component at its maximum amplitude. The differences in the measured damping levels indicated at M ≈ 15 are believed to be real, and although the problem is not understood, the measurements suggest that the damping derivatives at higher Mach numbers may have some dependence on the type of motion pattern experienced by the model. Within the band of amplitudes of the present measurements ($\bar{\delta}$ = 2.5 to 12 deg), no amplitude effect on damping was detected.

The two theoretical curves (Refs. 7 and 8) shown in Fig. 4 indicate a small increase in the damping derivatives with increasing Mach number, but this increase is not as large as that indicated by the experimental measurements. In view of the larger increase in the experimental damping values with Mach number than was expected, particular care was exercised in examining different factors that could have possibly affected the data; however, nothing has been found to invalidate the experimental measurements.

One potential error source that was considered in some detail was the effect of the geometry of the model nose changing during the flight owing to aerodynamic heating. At the higher Mach numbers, the shadowgrams of the model indicated that a slight change in nose bluntness occurred during flight, and in the worst case the R_N/R_B ratio increased to about 0.07 at the downrange end of the range. It has been noted in previous range testing that a copper nose tip at high heating conditions appears to melt, and a portion of the tip material is redistributed along the nose of the model immediately aft of the tip. In fact, it is questionable whether any mass is actually lost from copper nose models. Hence, any nose effect existing in the present measurements is believed to be related to the small change in nose geometry rather than to actual material ablation.

In an attempt to assess the effect of the small changes in nose geometry on the damping measurements, a series of shots was analyzed independently over the first half and over the second half of their flights. It follows that if nose geometry effects were large, they would be reflected in damping values reduced in this manner. The results of this analysis indicated no consistent difference in the reduced damping values obtained for the first and second portions of the individual flights. That is, the damping values obtained during the first portion of these flights were neither consistently higher nor lower than those for the second portion. Furthermore, the differences in the damping values computed for the first and second portions of the individual shots were always small relative to the experimentally observed increase in damping at the higher Mach numbers. It is also significant that, for shots at Mach numbers up through $M \approx 11$, no nose shape change was detectable; however, the data point at $M \approx 11$ is consistent with the trend established by the higher Mach number shots in indicating increased damping with Mach number.

Further indication of the negligible effect of nose geometry changes on the dynamic stability derivatives was obtained from the damping measurements for three shots using models with a larger initial bluntness ratio $((R_N/R_B) \approx 0.07)$, presented in Fig. 5. Nose shape changes for these models would necessarily be smaller than those for models with the sharper tip; however, these shots also show a similar trend of increasing damping with increasing Mach number. Also shown in Fig. 5 is a curve representing the data given in Fig. 4 for $(R_N/R_B) \approx 0.032$. It is of interest that the measurements do not indicate any significant effect of bluntness on damping, within the small bluntness change of the present tests.

4.2 STATIC STABILITY DERIVATIVES

In examining the $C_{m\alpha}$ data of the test program, it became apparent that $C_{m\alpha}$ was more sensitive to amplitude for some test conditions than had been anticipated. Hence, the amount of available data was not sufficient to define well the effects of amplitude on $C_{m\alpha}$ in some cases. However, certain variations of $C_{m\alpha}$ with amplitude are indicated in the limited number of range measurements, and these are discussed in detail. In this report, adjustments of $C_{m\alpha}$ data (either range or wind tunnel data) to another moment reference position were made using a $C_{N\alpha}$ value of 1.91.

Measured variations of $C_{m\alpha}$ with amplitude for $(R_N/R_B) \approx 0.032$, are shown in Fig. 6 for Mach numbers near 6, 11, and 15.5. A sectional curve fitting procedure wherein the equation of motion is fitted

to the motion data of different portions of a flight was used in some cases in reducing the $C_{m\alpha}$ data. The sectional fitting procedure is an aid in identifying amplitude effects in $C_{m\alpha}$ data for some test conditions.

Within the band of M, R_N/R_B, and Re_ℓ for the shots involved, the measurements at M ≈ 6 (Fig. 6a) indicate a near constant $C_{m\alpha}$ for mean amplitudes up to about 7 deg; whereas, at M ≈ 11 (Fig. 6b) a slight increase in $C_{m\alpha}$ with amplitude is indicated. It is believed that the variation in $C_{m\alpha}$ with amplitude, shown in Fig. 6b (note the $C_{m\alpha}$ variations for individual shots) is related to amplitude differences rather than to the differences in Reynolds number listed in Fig. 6b for the shots involved. The $C_{m\alpha}$ values presented in Fig. 6c for M ≈ 15.5 were measured over the first one-third portion of the range length because of the higher nose heating conditions associated with these shots, and any effects of possible nose geometry changes on the presented $C_{m\alpha}$ values are believed to be negligibly small. In general, the variation of $C_{m\alpha}$ was small for mean amplitudes up to about 16 deg; however, the data in Fig. 6c suggest an apparent slight shift in magnitude in the amplitude region near $\bar{\delta}$ = 10.5 deg (near the cone semiangle). Also shown in Fig. 6 are the Newtonian predicted levels of $C_{m\alpha}$ which are in reasonable agreement with the present measurements. It should be noted that the Newtonian theory as used in this paper is the unmodified Newtonian theory ($C_p = 2 \sin^2\delta_1$).

The faired $C_{m\alpha}$ curves of Fig. 6 are replotted in Fig. 7 and indicate that $C_{m\alpha}$ increases slightly with Mach number for mean amplitudes between about 3 and 7 deg.

Measured variations of $C_{m\alpha}$ as a function of $\bar{\delta}$ are shown in Fig. 8 for cones having larger bluntness ratios. The data for (R_N/R_B) ≈ 0.1, shown in Fig. 8c, were obtained in a previous Range G test program (Ref. 9). For comparison purposes, the faired $C_{m\alpha}$ curves of Fig. 8 are replotted in Fig. 9. Also shown in Fig. 9 is the faired $C_{m\alpha}$ curve of Fig. 6c for (R_N/R_B) ≈ 0.032 and M ≈ 15.5. The measurements indicate an appreciable decrease in $C_{m\alpha}$ for an increase in R_N/R_B from 0.032 to 0.07 at M ≈ 15. It is of significance that, at this Mach number, the limited amount of data indicates that the difference obtained in $C_{m\alpha}$ for the two values of (R_N/R_B) diminishes at the lower amplitudes and suggests the possibility that $C_{m\alpha}$ may be higher for the blunter cone at values of $\bar{\delta}$ near zero. At M ≈ 11, a $C_{m\alpha}$ level is observed similar to that at M ≈ 15, indicating that any Mach number effect on $C_{m\alpha}$ in this amplitude and Mach number range is small. The marked increase in $C_{m\alpha}$ $((R_N/R_B)$ = 0.07) noted for the lower amplitudes in the M ≈ 15 data is not evident in the M ≈ 11 data at comparable amplitudes. The M ≈ 9 data for (R_N/R_B) = 0.1 (from Ref. 9) show a

further decrease in $C_{m\alpha}$ below the level of the data for $M \approx 11$ and $M \approx 15$. This lower level in $C_{m\alpha}$ is believed to be associated primarily with the further increase in bluntness rather than with the Mach number difference because of the small Mach number effect noted previously in the data at $M \approx 15$ and $M \approx 11$. A marked increase in $C_{m\alpha}$ similar to that obtained at $M \approx 15$ is observed in the $M \approx 9$ data for amplitudes less than 4 deg. It appears from the experimental data of this figure that the amplitude associated with the increase in $C_{m\alpha}$, observed at smaller amplitudes, is Mach number dependent. Unfortunately, the absence of sufficient, low amplitude data at $M \approx 11$ precludes further confirmation of this observation. Within the assumption that any Mach number effect on $C_{m\alpha}$ is small, the present measurements indicate, for amplitudes in the range between 6 and 10 deg, that $C_{m\alpha}$ decreases with increasing bluntness for R_N/R_B values up to at least 0.1.

Values of $C_{m\alpha}$ obtained, for $\bar{\delta} = 7$ deg, from the curves of Fig. 9 and the level of $C_{m\alpha}$ obtained in a free-flight wind tunnel test at AEDC are shown in Fig. 10 as a function of bluntness ratio. Also shown in Fig. 10 are the variations of $C_{m\alpha}$ with bluntness ratio that are predicted by the Newtonian and the unsteady flow field theories which are for amplitudes near zero. The general trends of the theoretical curves are consistent with the decrease in $C_{m\alpha}$ indicated in the free-flight measurements for the small range of nose bluntness ratio, at $\bar{\delta} = 7$ deg. However, as noted previously, the present measurements for bluntness ratios of 0.07 and greater (see Fig. 9) suggest that, at amplitudes near zero, a nose bluntness may result in a greater $C_{m\alpha}$ than for a pointed cone. Further experimental evidence of this effect can be obtained from data presented in Ref. 10. The tests of Ref. 10 were at $M = 14$ and at amplitudes less than 2.8 deg, and the measured $C_{m\alpha}$ for a 10-deg semi-angle cone $(R_N/R_B) = 0.1$ was appreciably larger than the $C_{m\alpha}$ for a pointed cone; it should be noted that this comment is valid for $C_{m\alpha}$ measurements of Ref. 10 referenced to a common pivot axis position expressed as a percentage of actual model length from the nose.

In Fig. 11, $C_{m\alpha}$ values (adjusted to cg = 65) are shown as a function of Reynolds number. These measurements are for Mach numbers near 6. An examination of schlieren photographs indicated that the lowest data point of the group of data points near $Re_{\ell} = 4.8 \times 10^6$ corresponded to a shot that had a laminar boundary layer over the complete length of the model. This shot also had the lowest amplitude, $\bar{\delta} = 0.7$ deg. Schlieren photographs for other shots of this group (higher amplitudes) indicate that the location of transition was near the base of the model. Hence, the faired curve in Fig. 11 is believed to be representative of the variation of $C_{m\alpha}$ with Reynolds number for a cone having a laminar boundary layer. The limited measurements available at the higher

Reynolds numbers indicate that $C_{m\alpha}$ increases slightly as transition moves onto the cone.

4.3 LIFT- AND NORMAL-FORCE DERIVATIVES

The variations of $C_{L\alpha}$ and $C_{N\alpha}$ with amplitude, for $M = 6$ and over a Reynolds number range from 0.2×10^6 to 5×10^6, are shown in Fig. 12. The $C_{L\alpha}$ measurements decrease slightly with increasing $\bar{\delta}$ such that the corresponding $C_{N\alpha}$ values (for $(R_N/R_B) = 0.032$) are nearly constant for δ up to 6 deg. These data indicate that at $M = 6$ the effect of Reynolds number on $C_{L\alpha}$ and $C_{N\alpha}$ within the above Re_ℓ range is not significant. The $C_{N\alpha}$ level predicted by the Newtonian theory is also shown in Fig. 12b and is in good agreement with the present measurements.

Variations of $C_{L\alpha}$ and $C_{N\alpha}$ with amplitude, for $Re_\ell \approx 0.4 \times 10^6$, and for Mach numbers from 6 to 16, are shown in Fig. 13. The measurements shown in Figs. 13a and b indicate that, again, $C_{L\alpha}$ decreases with increasing amplitude such that the corresponding $C_{N\alpha}$ values (for $(R_N/R_B) \approx 0.032$) are nearly constant for $\bar{\delta}$ up to at least 18 deg. Further, the measurements indicate that both $C_{L\alpha}$ and $C_{N\alpha}$ tend to be insensitive to Mach number. The faired $C_{N\alpha}$ curve of Fig. 13b is replotted in Fig. 13c. Also shown in Fig. 13c are measurements for $(R_N/R_B) \approx 0.07$ and for $Re_\ell \approx 5 \times 10^6$. The limited number of measurements does not indicate any significant effects of either Reynolds number or of small nose bluntness on $C_{N\alpha}$. The $C_{N\alpha}$ levels predicted by the Newtonian theory, for $(R_N/R_B) = 0.032$ and 0.07, are also shown in Fig. 13 and are in good agreement with the present measurements.

4.4 CENTER OF PRESSURE

The variations of cp with Reynolds number, amplitude, and Mach number are shown in Fig. 14. The measurements in Fig. 14a, for $M \approx 6$ and for $\bar{\delta}$ up to about 6 deg, indicate that cp (for $(R_N/R_B) \approx 0.032$) tends to be insensitive to Reynolds number if the model has a laminar boundary layer. As stated previously, for $Re_\ell \approx 4.8 \times 10^6$, the location of transition for $M \approx 6$ is near the base of the model. The lowest data point (more forward cp) in the group of data points at Reynolds numbers near 4.8×10^6, corresponds to the shot noted in the discussion of the $C_{m\alpha}$ data of Fig. 11 and has the lowest amplitude, $\bar{\delta} = 0.7$ deg. Hence, this group of data points would suggest that the cp moves slightly rearward as transition moves onto the cone.

The cp measurements for $M \approx 15$ ($(R_N/R_B) \approx 0.032$, $Re_\ell \approx 0.4 \times 10^6$) are plotted as a function of amplitude in Fig. 14b. These data do not indicate any significant effect of amplitude on the cp.

Measurements in Fig. 14c, for $Re_\ell \approx 0.4 \times 10^6$ and for mean amplitudes from 5 to 12 deg, indicate that cp (for $(R_N/R_B) \approx 0.032$) moves slightly rearward with increasing Mach number. The cp measurements for $(R_N/R_B) \approx 0.07$, also shown in Fig. 14c, are in general agreement with the cp values for the sharper cone; the lower data point (triangular symbol) at $M \approx 11$ is believed to be lower because of the higher amplitude ($\bar{\delta} \approx 11.5$ deg) of this shot in combination with the larger bluntness ratio.

The levels of cp predicted by the Newtonian theory are also shown in Fig. 14 and are in reasonable agreement with the present measurements.

4.5 DRAG COEFFICIENT

Drag coefficient, C_{D_O}, is presented as a function of Mach number in Fig. 15 for $Re_\ell \approx 0.4 \times 10^6$. Measurements indicate that C_{D_O}, for $(R_N/R_B) \approx 0.032$, decreases with increasing Mach number. Additional drag measurements shown in Fig. 15 for bluntness ratios from 0.02 to 0.07 indicate that C_{D_O} tends to be insensitive to small changes in nose bluntness.

Some C_{D_O} measurements, for $M \approx 6$, are shown as a function of Reynolds number in Fig. 16. The lowest data point in the group of data points near $Re_\ell = 4.8 \times 10^6$ corresponds to the same shot noted in the discussion of the C_{m_α} data of Fig. 11. It was noted then that this shot had the minimum amplitude, $\bar{\delta} = 0.7$ deg, and that the schlieren photograph for this shot indicated that the model had a laminar boundary layer over its entire length. Hence, the faired curve in Fig. 16 is believed representative of the C_{D_O} variation for the case of the cone having a laminar boundary layer.

The variation of C_{D_O} as transition moves onto the cone is not defined adequately in the present tests, partially because of the sensitiveness of the location of transition with small amplitude changes; however, the measurements at the higher Reynolds numbers indicate an appreciable increase in C_{D_O} as transition moves onto the cone.

Measurements of C_{D_O} for $(R_N/R_B) \approx 0.1$, as a function of Reynolds number, are shown in Fig. 17. Additional data points for $(R_N/R_B) \approx 0.032$ and 0.08 indicate that effects of small changes in nose bluntness on C_{D_O} are not significant for these test conditions.

SECTION V
COMPARISON OF RANGE DATA WITH WIND TUNNEL DATA

Comparisons of the present range measurements with wind tunnel data are shown in Figs. 18 through 23. The faired $C_{m\alpha}$ curve (M ≈ 6) of Fig. 11, corresponding to a condition of a laminar boundary layer, is replotted in Fig. 18. Also shown in Fig. 18 are $C_{m\alpha}$ measurements for a sting-supported 10-deg semiangle cone obtained at the Jet Propulsion Laboratory (JPL) (Ref. 11) for similar test conditions. The JPL measurements have been adjusted to a moment reference at 65 percent of the cone length from the nose. The significance of this data comparison is related to the different trends exhibited in the two sets of data. The JPL measurements increase appreciably with decreasing Reynolds number, whereas the range measurements are nearly constant. The difference in absolute magnitude of $C_{m\alpha}$ between the two sets of measurements is of no concern because of the different nose bluntness ratios (indicated in Fig. 18) that are involved.

In Fig. 19, a comparison is made between the range damping data (faired curve replotted from Fig. 3) for M ≈ 6 and damping measurements obtained in the JPL tests (Ref. 11). The range measurements indicate somewhat more damping than measured in the JPL tests. In consideration of previous comments regarding nose bluntness effects on damping, the effect of the small difference in R_N/R_B existing in the data shown in Fig. 19 would be expected to be negligibly small.

The motion plot shown in Fig. 20 corresponds to the shot at a Reynolds number of 3.2×10^6 (see Figs. 3 and 11); hence, this shot was one of those used in defining the range variations of $C_{m\alpha}$ and $C_{mq} + C_{m\dot{\alpha}}$ shown in Figs. 18 and 19. The quality of this motion plot (better than for some shots) is such that an examination of the plot aids in assuring the reasonableness of the range measurements of Figs. 18 and 19. It can be observed in Fig. 20 that the fitted curve describes the variation of the measured β values very well. The roll rate for this shot was near zero; hence, the damping of the model can be evaluated from the decay of either the β or α motion component of the yawing motion, and $C_{m\alpha}$ can be evaluated from the wavelength of either the β or α motion component. In general, the wavelength of the yawing motion of a model can be determined better than the amplitude decay. However, it is apparent from Fig. 20 that the error in evaluating the amplitude decay (proportional to the error in the measured damping) from the computer fitted curve, would be expected to be less than five percent.

A comparison of the range damping level at M = 10 with wind tunnel data obtained at AEDC at the same Mach number and over a range of cg position is shown in Fig. 21. Two theoretical curves are also shown in Fig. 21 to indicate the predicted trend of the damping derivatives with cg position. The wind tunnel data include results from free-flight models (at AEDC) and both gas-bearing-mounted and flexure-mounted, sting-supported models (AEDC), all tested in the same wind tunnel at similar flow conditions. Also included are measurements (using a flexure pivot), taken from Ref. 12, made at a single cg position and at three different frequencies.

Both range and tunnel free-flight dynamic stability measurements tend to be larger than the measurements for the sting-mounted models. These free-flight measurements in the range and wind tunnel tend to be consistent with one another, although there is a difference in Reynolds numbers between the two sets of measurements ($Re_\ell \approx 0.4 \times 10^6$ and 10^6 for the range and tunnel tests, respectively).

The Ref. 12 data, at a Re_ℓ comparable to the range data, indicate a frequency effect on damping, as shown in Fig. 21. It should be noted that apparent frequency effects on dynamic stability measurements have been observed in other tunnel tests. The portion of the Ref. 12 measurements which were obtained at frequencies comparable to the free-flight data in Fig. 21 indicate considerably less damping than the free-flight data. The portion of the Ref. 12 data band which appears to agree, in general, with the magnitude of the free-flight data in the figure is for an appreciably higher oscillation frequency than that corresponding to the free-flight data. On this basis, the frequency effect indicated in the data of Ref. 12 appears to be inconsistent with the range and tunnel free-flight measurements.

In Fig. 22, a comparison is made of the range $C_{m\alpha}$ data and wind tunnel data (involving sting-supported models) for high Mach numbers obtained from different facilities (Ref. 13 and AEDC (VKF) and Ling-Temco-Vought, Dallas, Texas). The solid curve in Fig. 22 corresponds to range $C_{m\alpha}$ values obtained from the curves of Fig. 7 at $\bar{\delta}$ = 5 deg. The $\bar{\delta}$ of 5 deg is a reasonable mean value of the amplitude band involved in the different sets of data shown in Fig. 22. The range $C_{m\alpha}$ curve (Fig. 22) is representative of a Reynolds number comparable to the different sets of wind tunnel data shown in Fig. 22; however, the range measurement at M ≈ 9.6 and Re_ℓ = 4.8 x 10^6 shown in Fig. 22 fails to indicate any significant effect of Reynolds number on $C_{m\alpha}$. From considerations of the nose bluntness differences noted in Fig. 22, the tunnel measurements would be expected to be higher than the range measurements; hence, the lower $C_{m\alpha}$ level indicated in the tunnel measurements at the higher Mach numbers is not understood. However, as

indicated in Fig. 22, the reduced frequency parameter, $\omega d/2V$, was higher in the tests corresponding to the lower $C_{m\alpha}$ values. Further, the cause of the difference in the $C_{m\alpha}$ measurements from the different facilities at $M \approx 14.2$ is not apparent.

In Fig. 23, a comparison is made of range damping data (faired curve replotted from Fig. 4) and wind tunnel damping data for high Mach numbers obtained from different facilities (Refs. 12 through 14); the tunnel tests involved sting-supported models. Again, the range free-flight damping measurements are, in general, higher than the tunnel measurements. It should be noted that Re_ℓ was similar for all data shown and that the pivot axis location in the tunnel tests was always more forward than the cg position of the models involved in the range tests. There is considerable spread in the frequencies associated with tunnel tests, but there is no consistent frequency effect observed which could account for the large difference existing between the range and tunnel damping measurements.

SECTION VI
CONCLUDING REMARKS

A free-flight range investigation of the stability and drag of a 10-deg semiangle cone was made at Mach numbers from 6 to 16. The measurements indicate that the damping of the cone increases appreciably with increasing Mach number between M = 8 and 16 at a Re_ℓ of about 0.4×10^6. Also, $C_{m\alpha}$ for the cone decreases significantly as the R_N/R_B ratio is increased up to 0.1 for amplitudes greater than about 5 deg.

Comparisons of the range stability data with wind tunnel data involving sting-supported models in different test facilities indicate that appreciable differences exist in the measurements. The cause of the differences in the range and tunnel stability data noted in this paper is not completely understood. It appears that tunnel support effects are one possible explanation for these differences.

REFERENCES

1. Hobbs, R. B., Jr. "Hypersonic Dynamic Stability, Part II. Conical Body Experimental Program." FDL-TDR-64-149, Part II, January 1967.

2. Nicolaides, John D. "On the Free Flight Motion of Missiles Having Slight Configurational Asymmetries." BRL Report No. 858, June 1953.

3. Murphy, C. H. "Data Reduction for the Free Flight Spark Ranges." BRL Report No. 900, February 1954.

4. Murphy, C. H. "Free Flight Motion of Symmetric Missiles." BRL Report No. 1216, July 1963.

5. Welsh, C. J. and Watt, R. M. "Effects of Roll on the Free-Flight Motion of Statically Stable Bodies." AEDC-TR-67-156 (AD658433), September 1967.

6. Shinbrot, Marvin. "A Least Squares Curve Fitting Method with Applications to the Calculation of Stability Coefficients from Transient-Response Data." NACA-TN-2341, April 1951.

7. Sauerwein, H. "Application of the Piston Analogy to the Calculation of Stability Derivatives for Pointed Axially Symmetric Bodies at High Mach Numbers." RAD-TM-61-40, October 1961.

8. Brong, E. A. "The Unsteady Flow Field about a Right Circular Cone in Unsteady Flight." FDL-TDR-64-148, January 1967.

9. Rogers, T., Giesecke, A. H., and Hammitt, A. G. "A Fluid Ejection System for Ballistic Range Testing." AIAA Paper No. 68-19, January 1968.

10. Clay, James T. "Nose Bluntness, Cone Angle, and Mach Number Effects on the Stability Derivatives of Slender Cones." ARL 67-0185, September 1967.

11. Prislin, Robert H. "High-Amplitude Dynamic-Stability Characteristics of Blunt 10-Degree Cones." JPL Technical Report No. 32-1012, October 1966.

12. Urban, R. H. "A Dynamic Stability Balance for Hypervelocity (Hotshot) Tunnels." AEDC-TR-65-222 (AD472707), October 1965.

13. Walchner, Otto, et al. "Hypersonic Stability Derivatives for a Standard 10 Degree Cone." ARL 67-0099, May 1967.

14. Urban, R. H. and Shanahan, R. J. "Dynamic Stability Characteristics of a 10-deg Cone at Mach Number 20." AEDC-TR-65-80 (AD461260), April 1965.

15. Rie, H., Linkiewicz, E. A., and Bosworth, F. D. "Hypersonic Dynamic Stability Part III, Unsteady Flow Field Program." FDL-TDR-64-149 Part III (AD650879), January 1967.
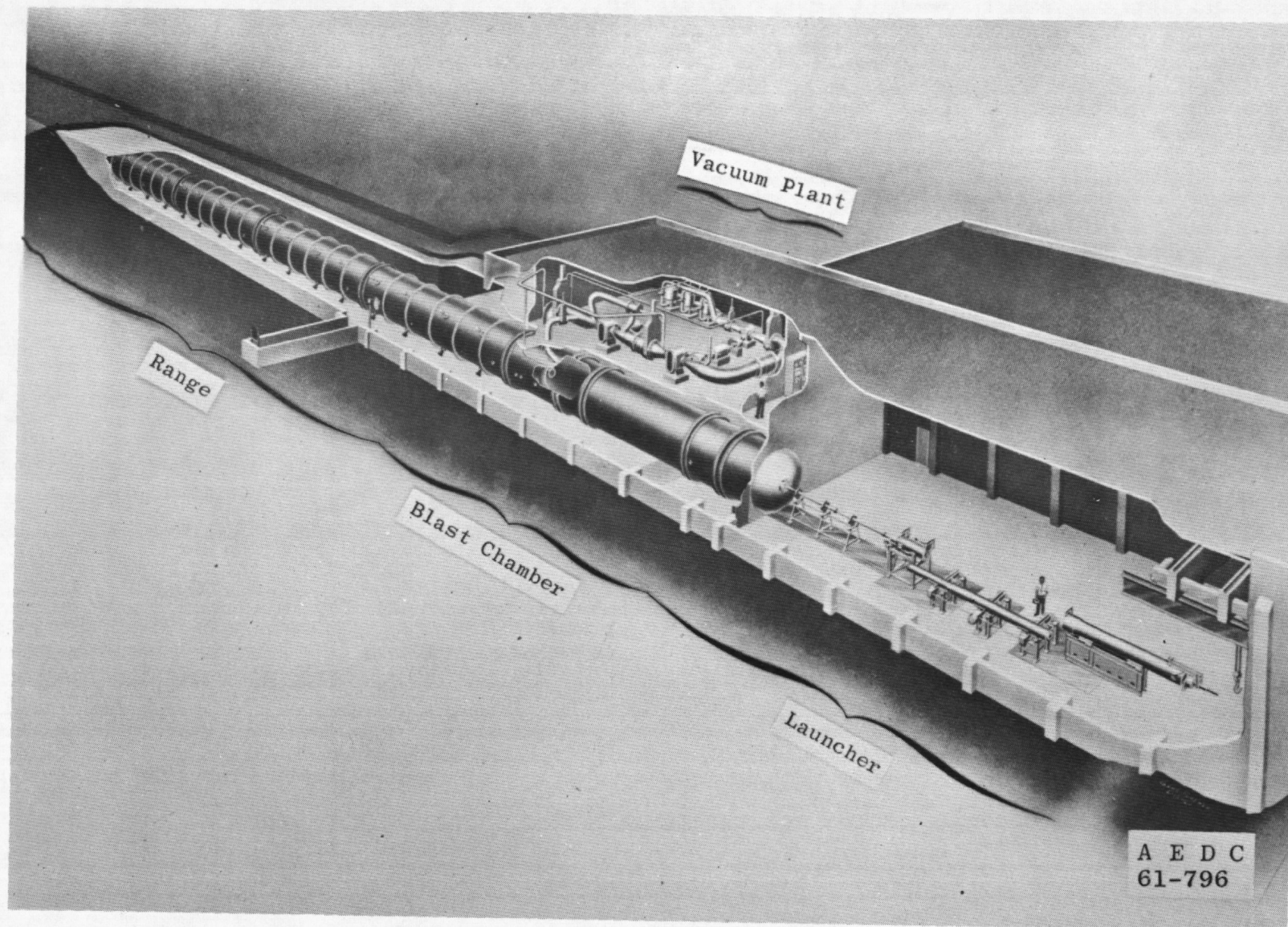
APPENDIX
ILLUSTRATIONS

Vacuum Plant
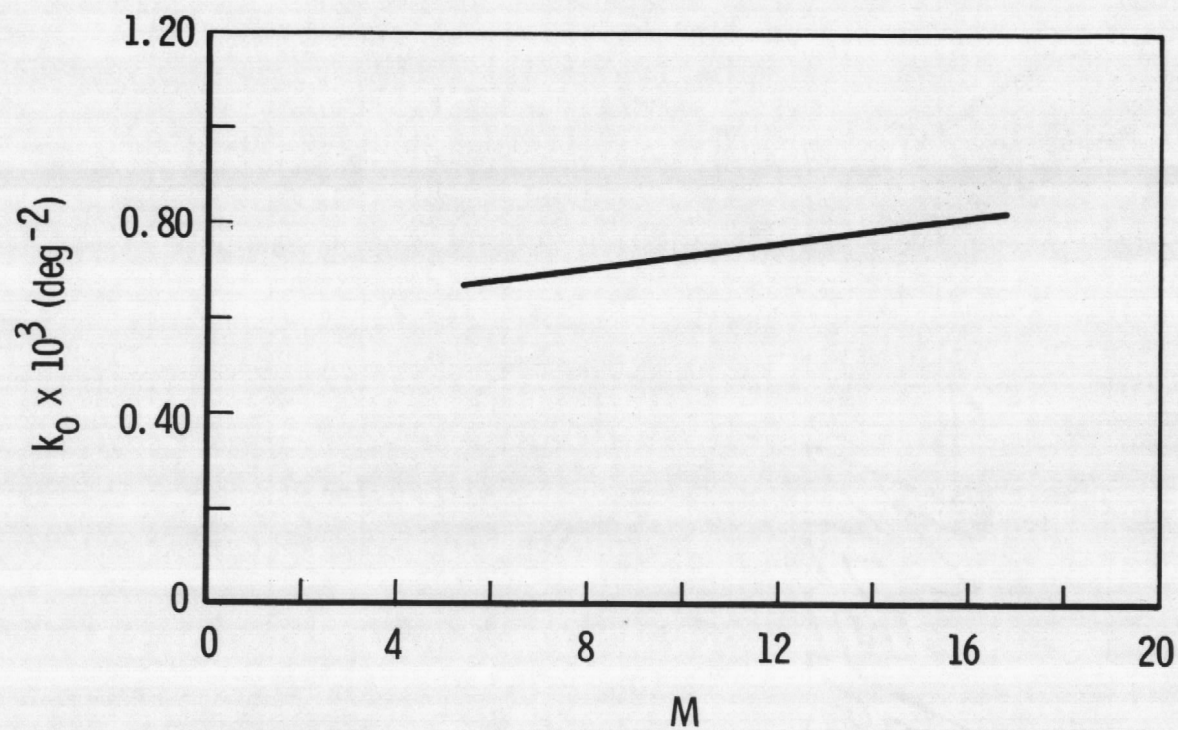
Range

Blast Chamber

Launcher

A E D C
61-796

Fig. 1 Range G
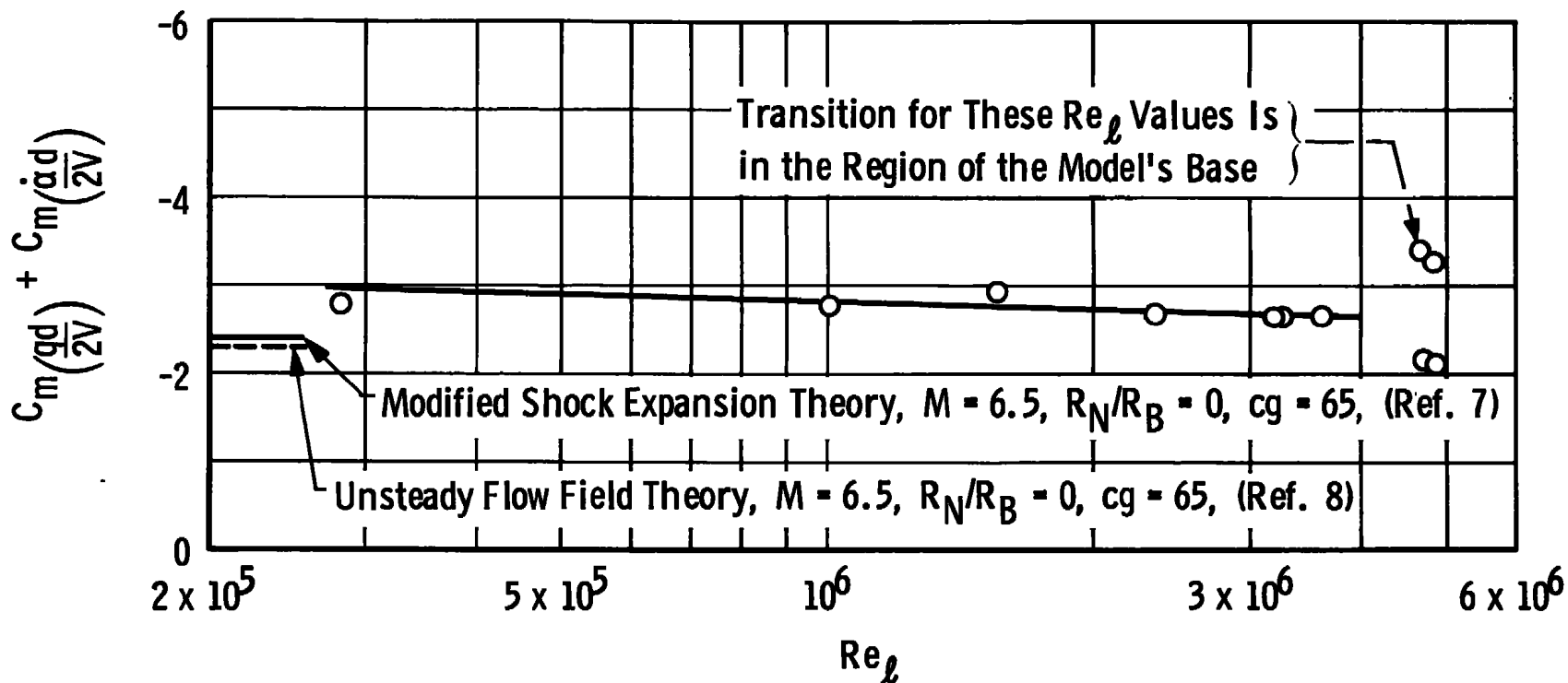
Fig. 2 Variation of the Drag Parameter, k_o, with Mach Number

Fig. 3 Damping-in-Pitch Derivatives for M ≈ 6.5

Range G

$Re_\ell = 0.38 \times 10^6$ to 0.45×10^6

$R_N/R_B \approx 0.032,$ $cg \approx 63$

$\omega d/2V = 0.0010$ to 0.0018

$\bar{\delta} = 2.5$ to 12.0 deg

---- Modified Shock Expansion Theory, $\theta_c = 10$ deg, $R_N/R_B = 0,$ $cg = 63$ (Ref. 7)

—·— Unsteady Flow Field Theory, $\theta_c = 10$ deg, $R_N/R_B = 0,$ $cg = 63$ (Ref. 8)

Different Symbols Indicate Gross
Change in Motion Patterns – See Text
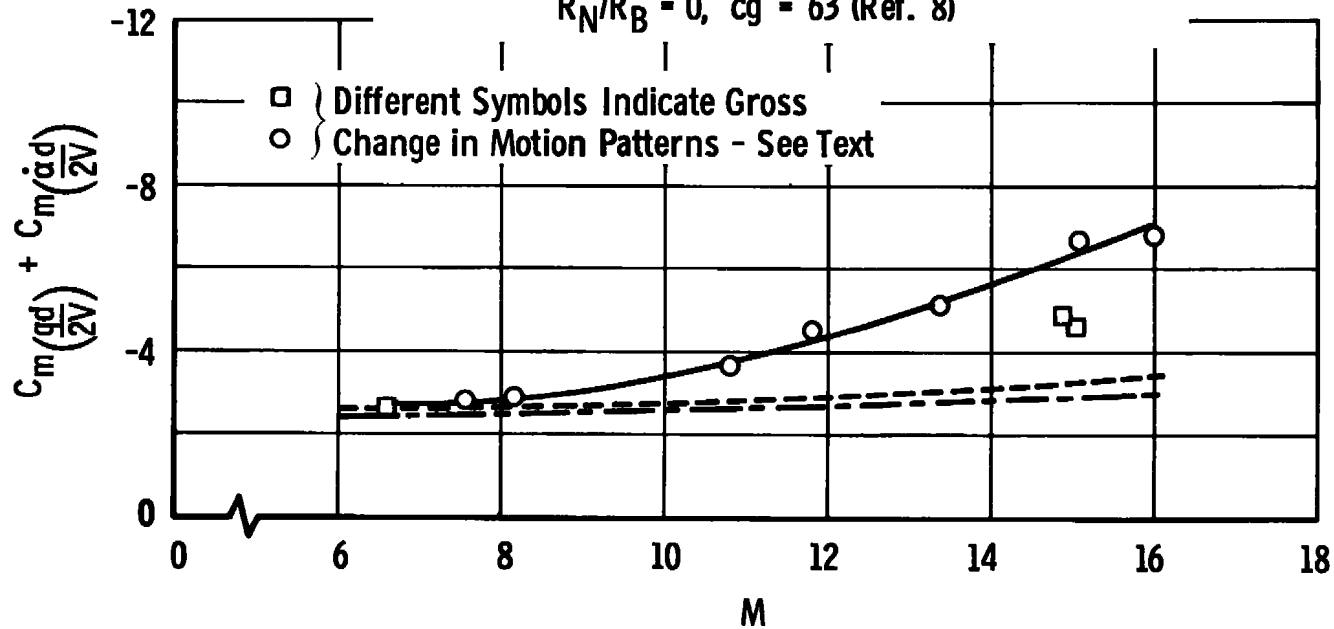
Fig. 4 Damping-in-Pitch Derivatives for $Re_\ell \approx 0.4 \times 10^6$
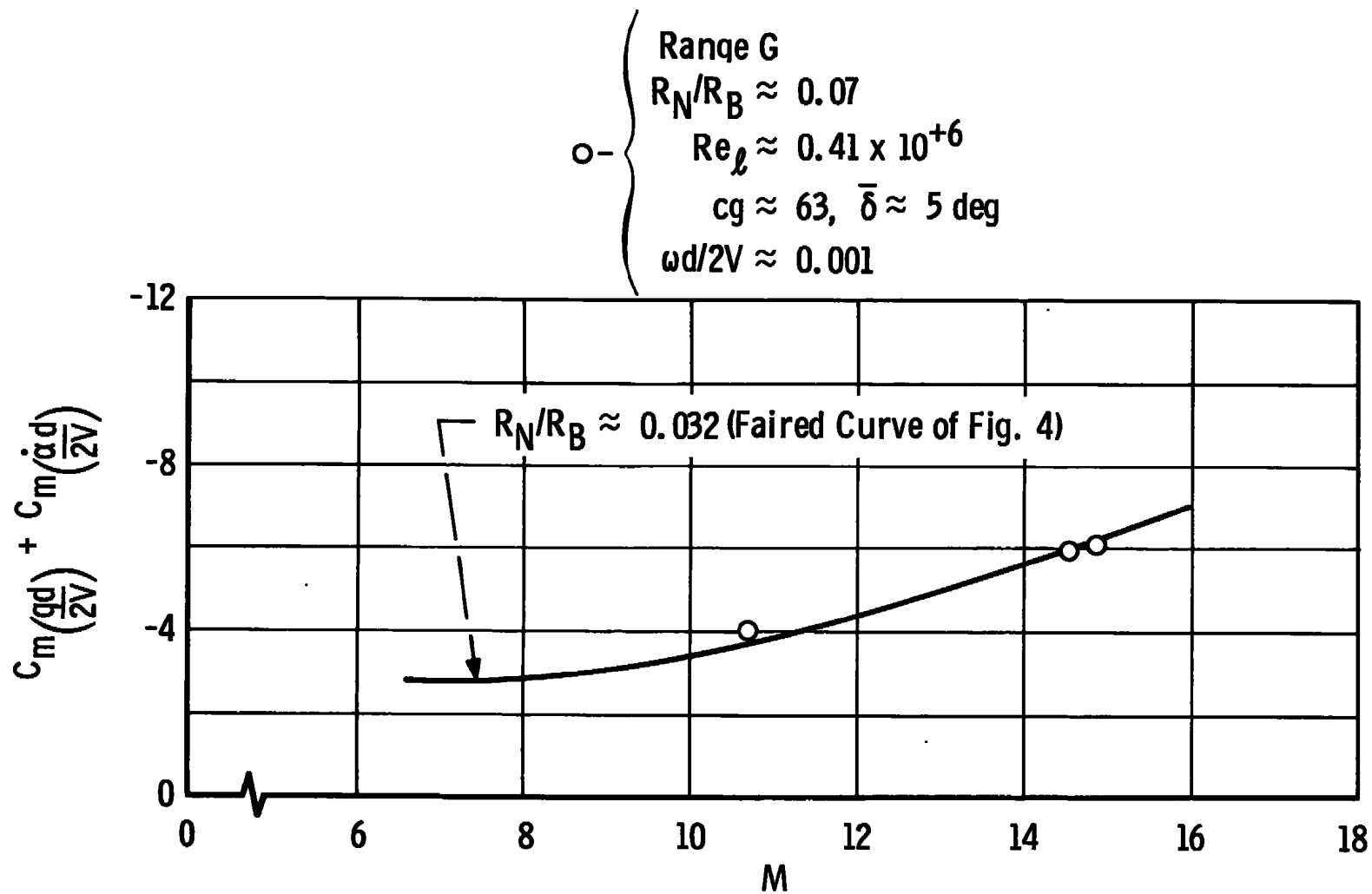
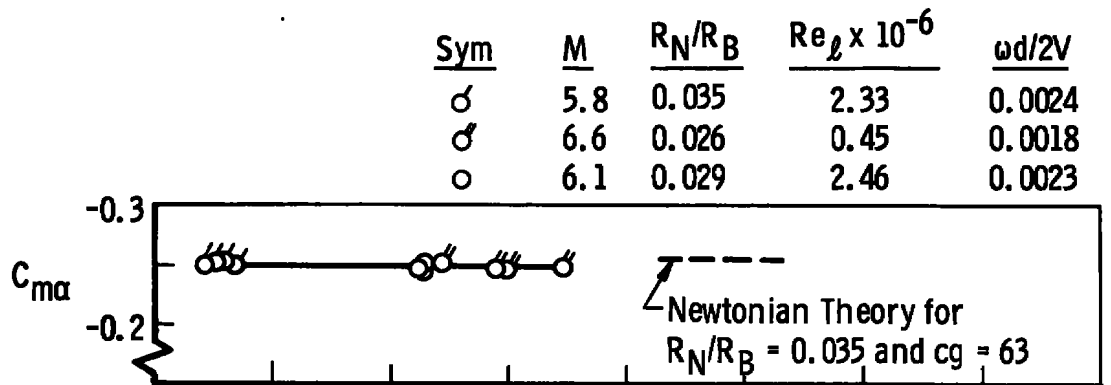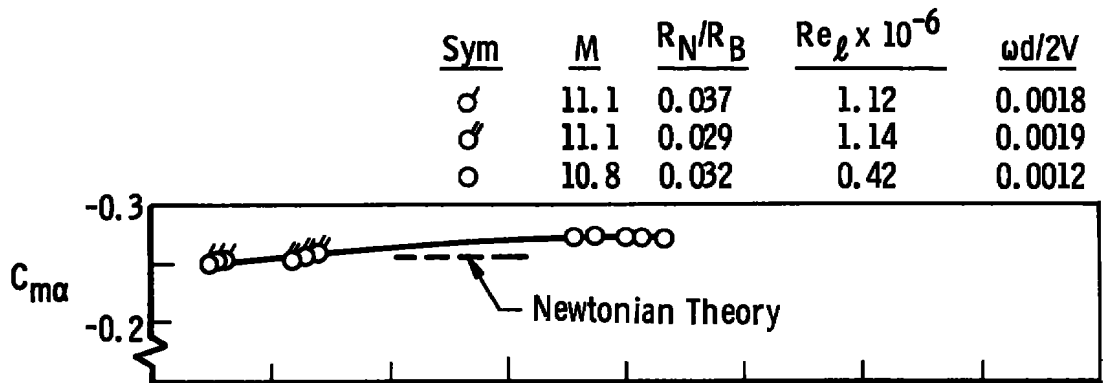Fig. 5 Damping-in-Pitch Derivatives for Different Nose Bluntness Ratios
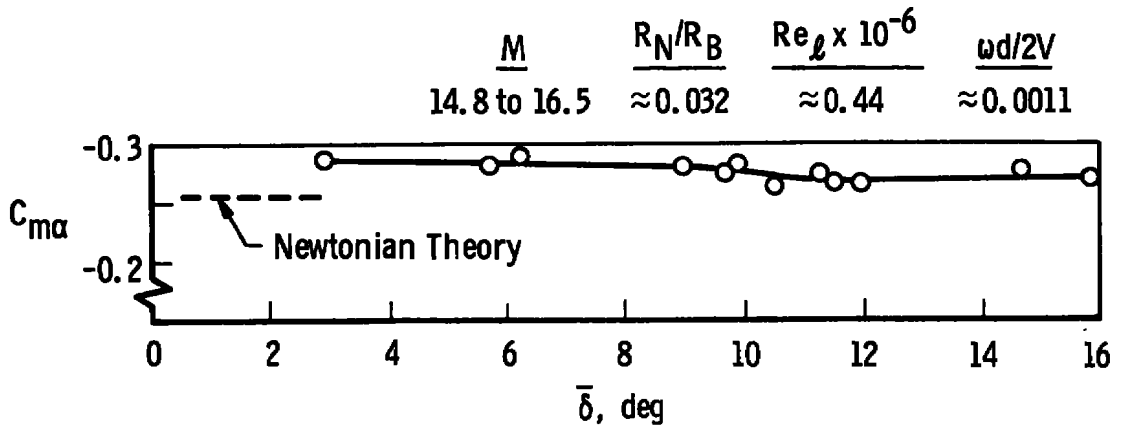
Sym	M	R_N/R_B	$Re_\ell \times 10^{-6}$	$\omega d/2V$
♂	5.8	0.035	2.33	0.0024
♂	6.6	0.026	0.45	0.0018
o	6.1	0.029	2.46	0.0023

a. M ≈ 6

Sym	M	R_N/R_B	$Re_\ell \times 10^{-6}$	$\omega d/2V$
♂	11.1	0.037	1.12	0.0018
♂	11.1	0.029	1.14	0.0019
o	10.8	0.032	0.42	0.0012

b. M ≈ 11

M	R_N/R_B	$Re_\ell \times 10^{-6}$	$\omega d/2V$
14.8 to 16.5	≈0.032	≈0.44	≈0.0011

c. M ≈ 15.5

Fig. 6 Static Stability Parameter as a Function of Amplitude for
R_N/R_B ≈ 0.032 (Data Adjusted to cg = 63)

Range G

$Re_\ell = 0.40 \times 10^6$ to 2.46×10^6

$R_N/R_B \approx 0.032$, cg = 63

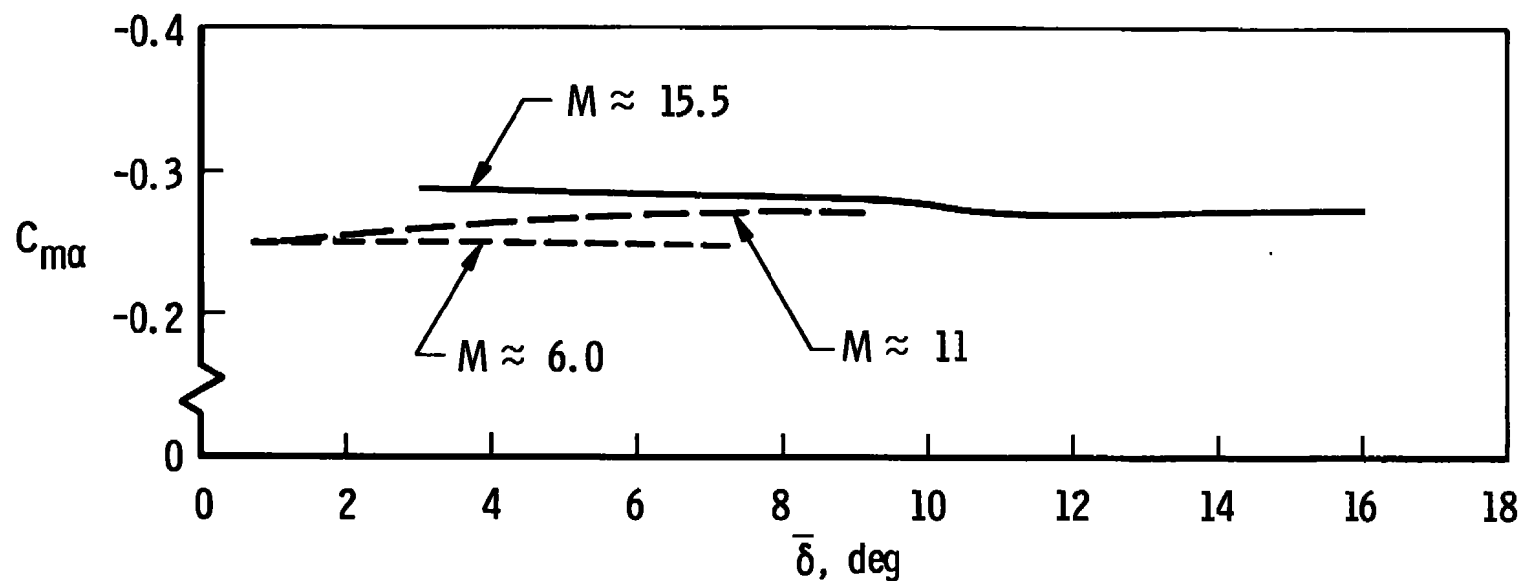$\omega d/2V = 0.0010$ to 0.0024

Curves Obtained from Fig. 6
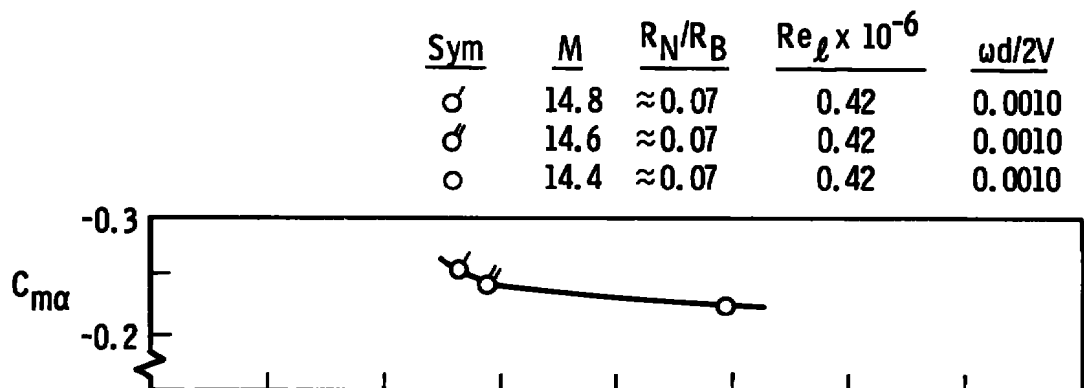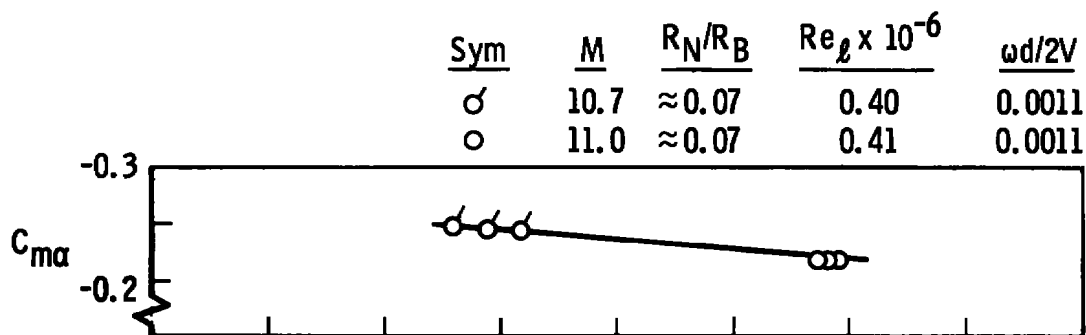

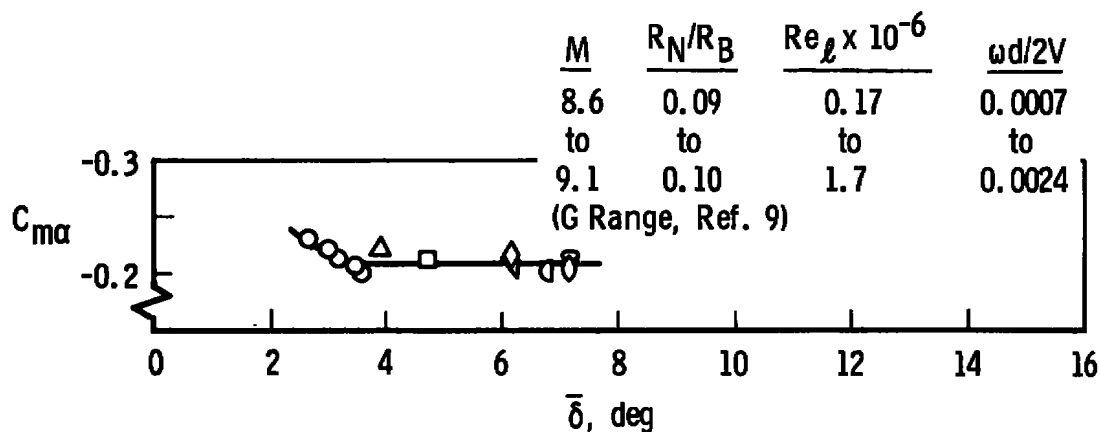Fig. 7 Comparison of $C_{m\alpha}$ Variations for Three Mach Numbers

Note: Different Symbols Indicate
Different Shots

Sym	M	R_N/R_B	$Re_\ell \times 10^{-6}$	$\omega d/2V$
♂	14.8	≈0.07	0.42	0.0010
♂	14.6	≈0.07	0.42	0.0010
○	14.4	≈0.07	0.42	0.0010

a. M ≈ 15

Sym	M	R_N/R_B	$Re_\ell \times 10^{-6}$	$\omega d/2V$
♂	10.7	≈0.07	0.40	0.0011
○	11.0	≈0.07	0.41	0.0011

b. M ≈ 11

M	R_N/R_B	$Re_\ell \times 10^{-6}$	$\omega d/2V$
8.6	0.09	0.17	0.0007
to	to	to	to
9.1	0.10	1.7	0.0024

(G Range, Ref. 9)

c. M ≈ 9

Fig. 8 Static Stability Parameter as a Function of Amplitude for (R_N/R_B) ≈ 0.07 and 0.1 (Data Adjusted to cg ≈ 63)

Range G

$Re_{\ell} = 0.17 \times 10^6$ to 1.7×10^6

$cg = 63$, $\omega d/2V = 0.001$ to 0.002

Curves Obtained from Figs. 6 and 8

$M \approx 15.5$, $R_N/R_B \approx 0.032$

$M \approx 11$, $R_N/R_B \approx 0.07$

$M \approx 9.0$, $R_N/R_B \approx 0.10$
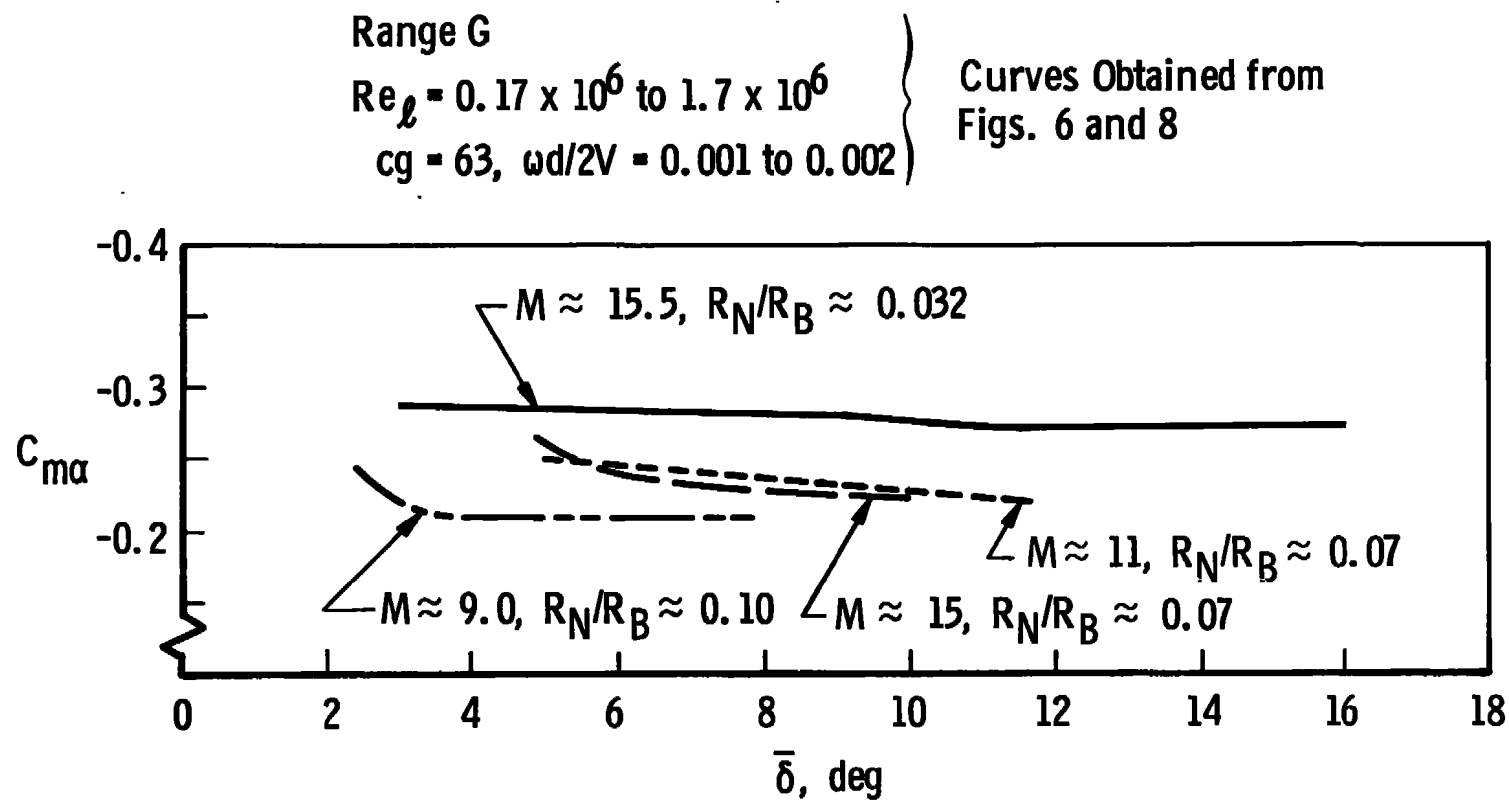
$M \approx 15$, $R_N/R_B \approx 0.07$

$C_{m\alpha}$

$\bar{\delta}$, deg

Fig. 9 Comparison of $C_{m\alpha}$ Values for Different Bluntness Ratios

△ $M \approx 15.5$

I $M \approx 11$ to 14.5 } From Fig. 9, $\bar{\delta} = 7$ deg

◊ $M \approx 9$

○ AEDC Wind Tunnel Free-Flight,
$M = 10$, $Re_{\ell} = 10^6$, $\omega d/2V = 0.003$
(Moment Reference Adjusted from
55 percent ℓ)
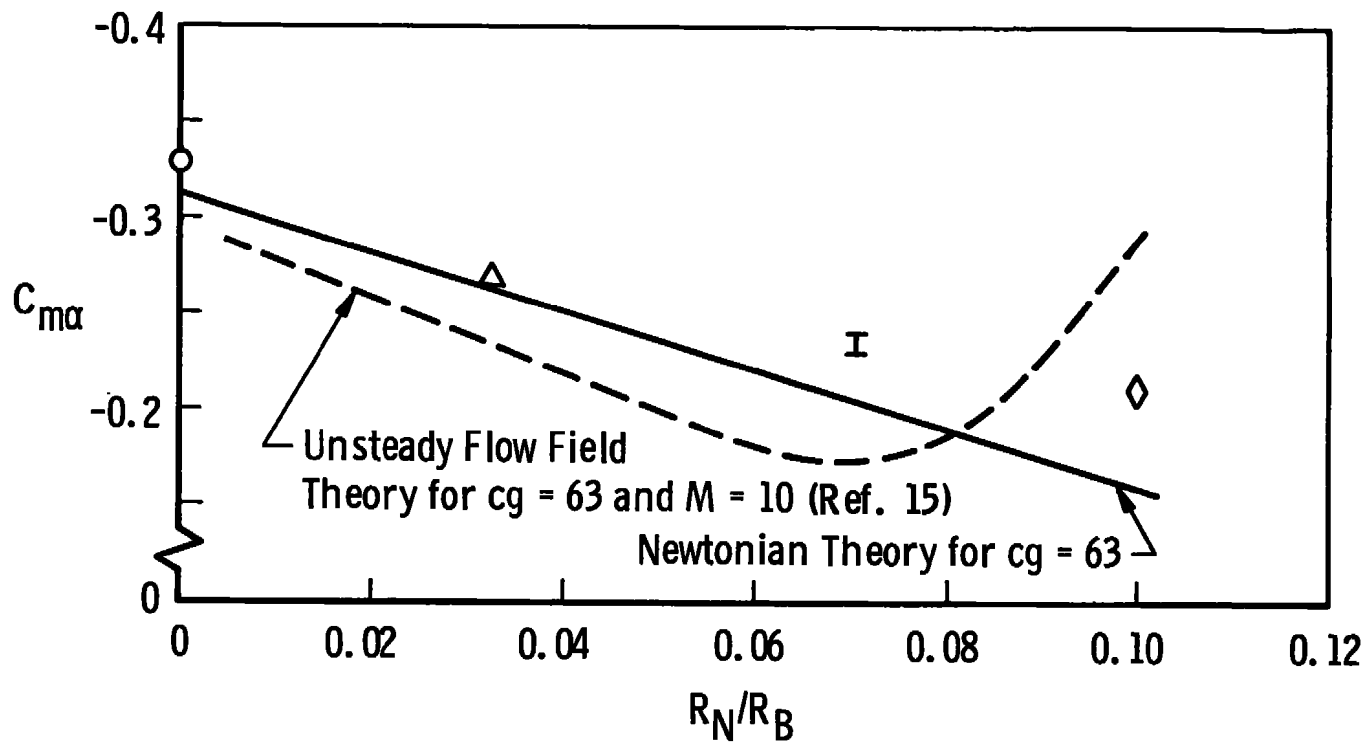
Fig. 10 Variation of $C_{m\alpha}$ with Bluntness Ratio for $\delta = 7$ deg (Moment Reference at 63 percent ℓ)

Range G
$M = 5.40$ to 6.50
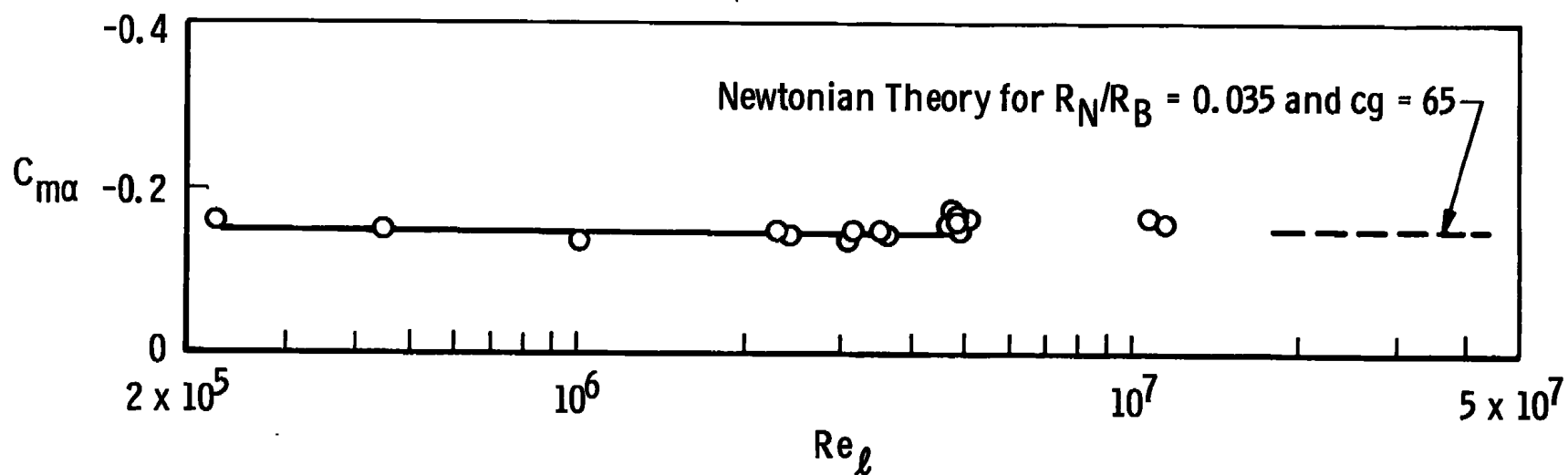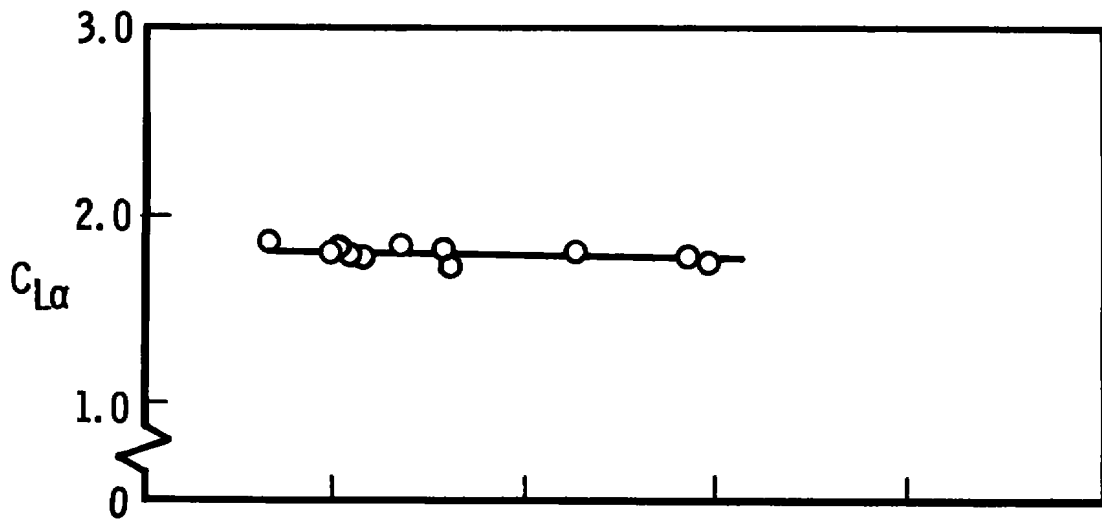$R_N/R_B \approx 0.032$, cg = 65
$\omega d/2V = 0.0012$ to 0.0032
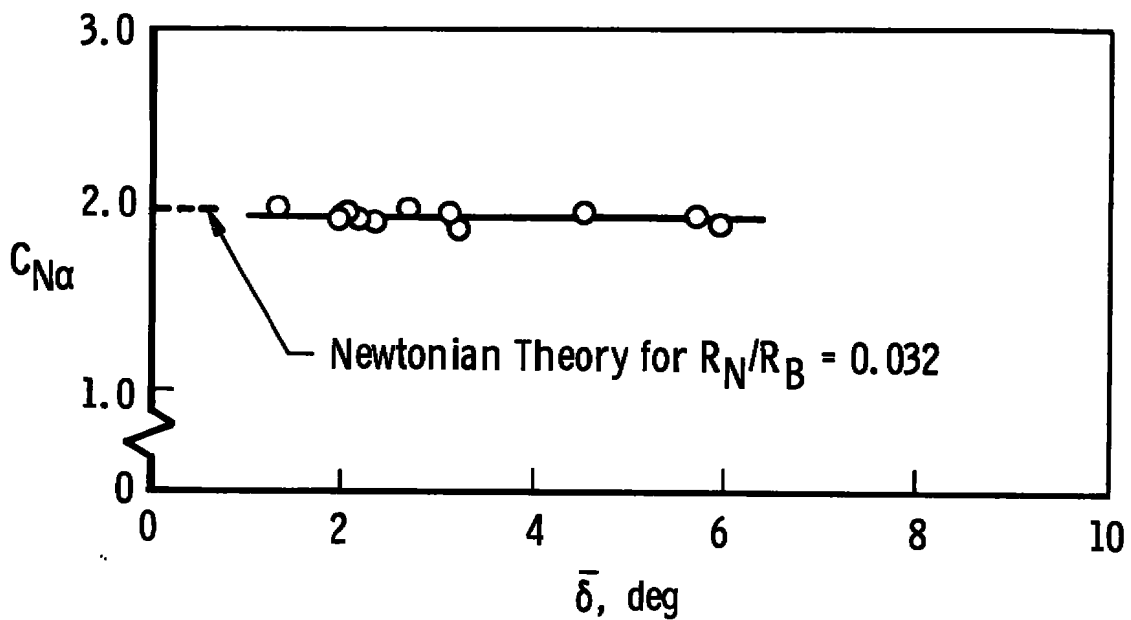$\overline{\delta} = 1$ to 10 deg

Newtonian Theory for $R_N/R_B = 0.035$ and cg = 65

$C_{m\alpha}$

Re_ℓ

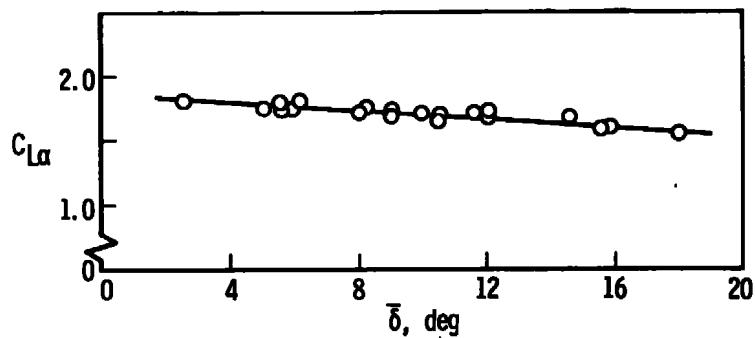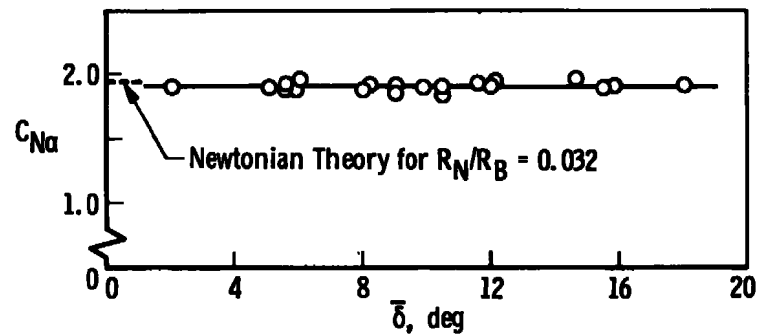Fig. 11 Variation of $C_{m\alpha}$ with Re_ℓ for $M = 6$

a. Lift-Force Derivative

b. Normal-Force Derivative

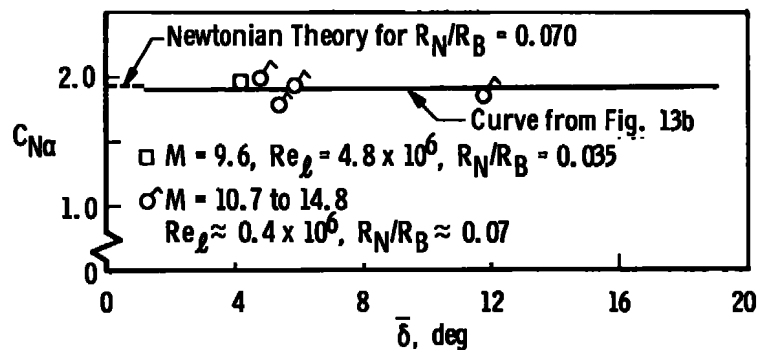Fig. 12 Variation of the Lift- and Normal-Force Derivatives with Amplitude ($M \approx 6$)

a. Lift-Force Derivative

b. Normal-Force Derivative

c. Normal-Force Derivative

Fig. 13 Variation of Lift- and Normal-Force Derivative with Amplitude
(M = 6 to 16)

a. $M \approx 6$, $R_N/R_B \approx 0.032$, $\bar{\delta} = 1$ to 6 deg

b. $M = 14.5$ to 15.8, $R_N/R_B \approx 0.032$, $Re_\ell \approx 0.4 \times 10^6$

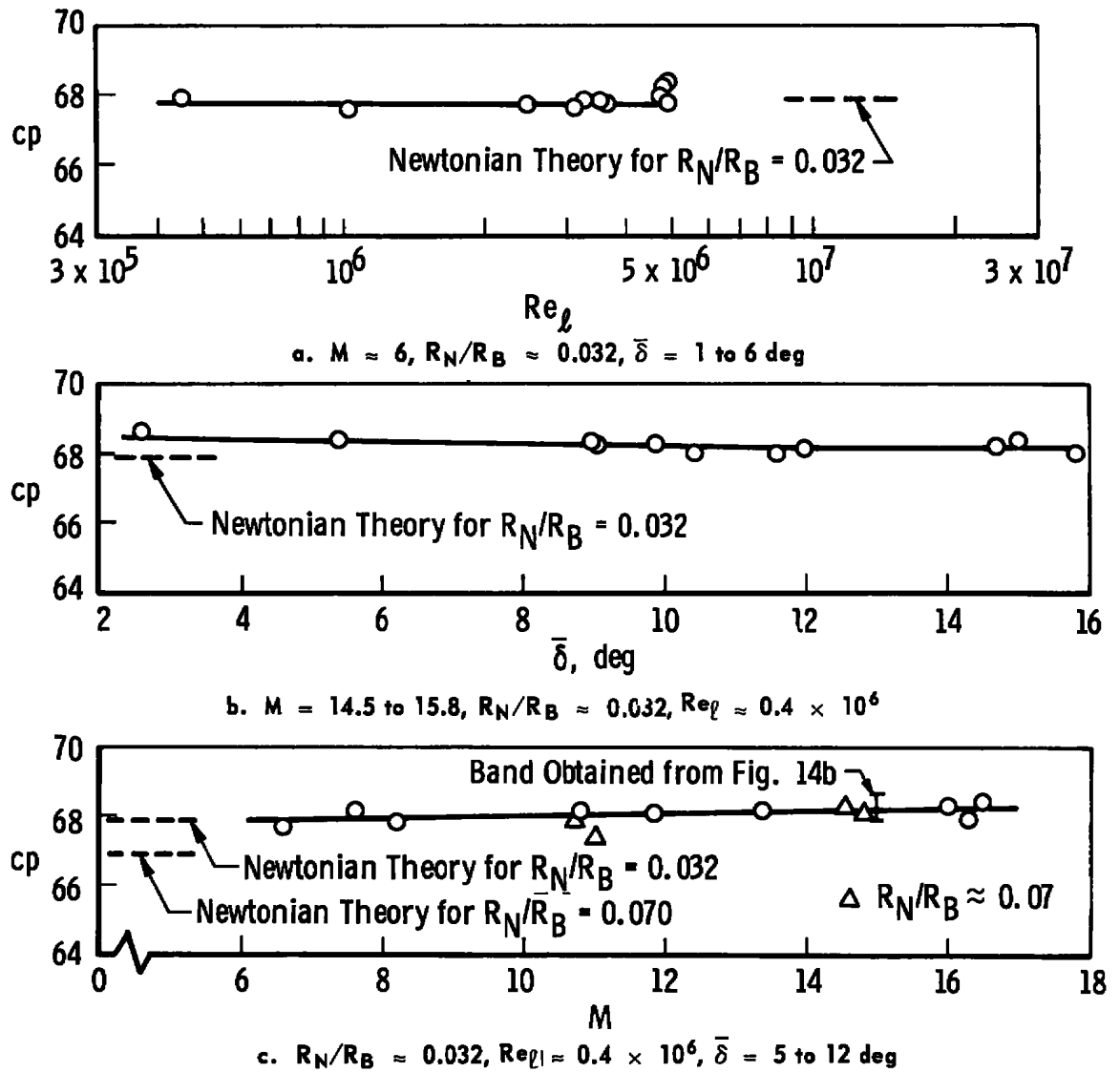c. $R_N/R_B \approx 0.032$, $Re_{\ell l} \approx 0.4 \times 10^6$, $\bar{\delta} = 5$ to 12 deg

Fig. 14 Center of Pressure as a Function of Reynolds Number, Amplitude, and Mach Number
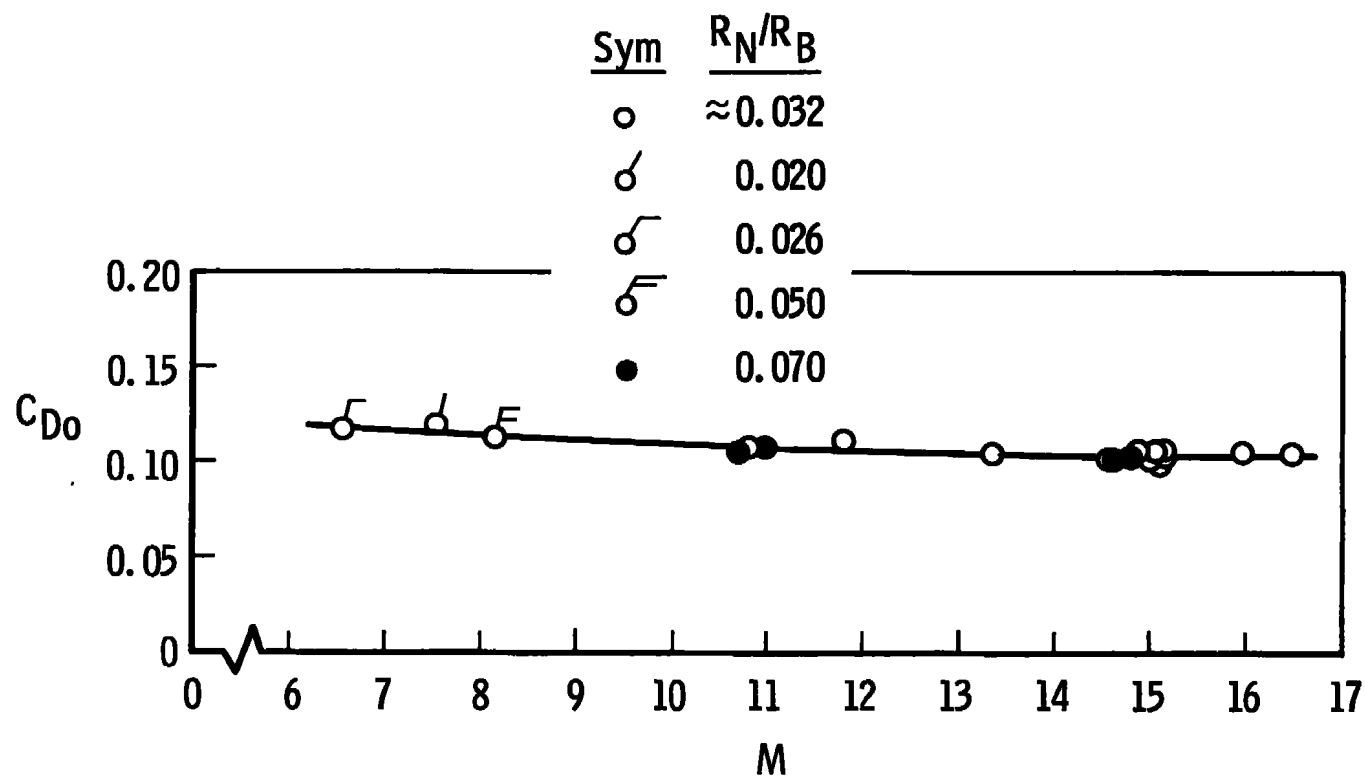
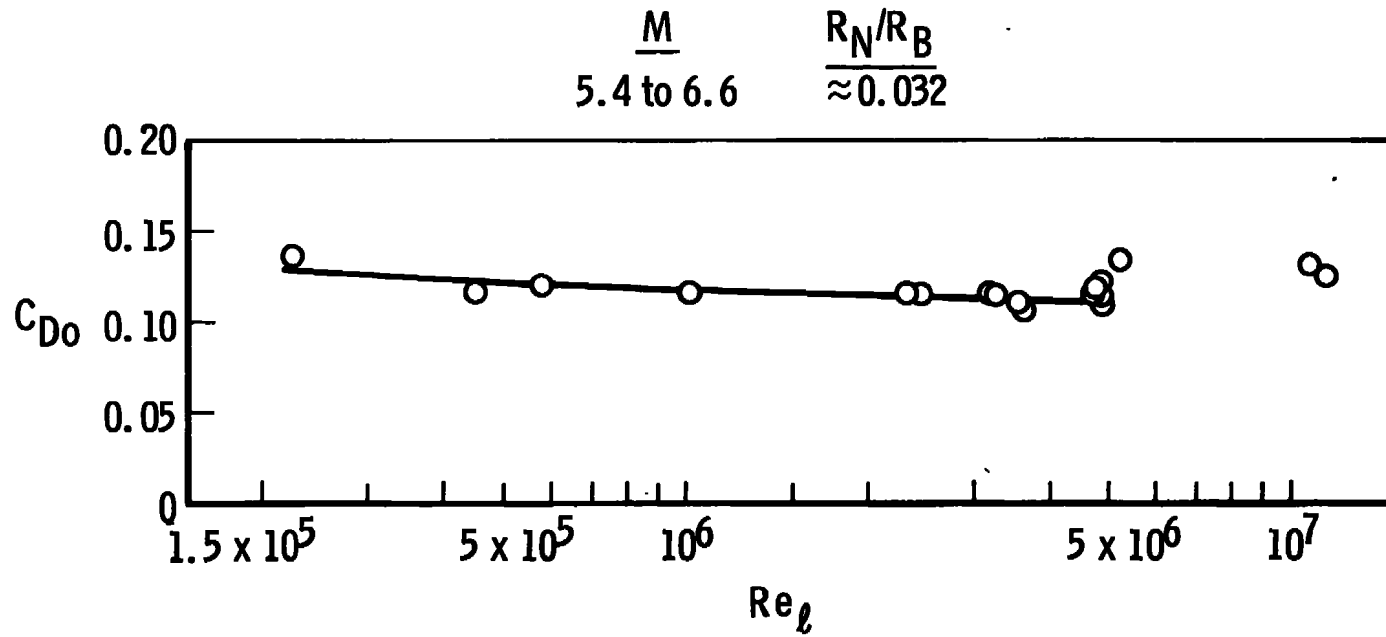Fig. 15 Drag Coefficient as a Function of Mach Number (Re$_\ell$ ≈ 0.4 × 10⁶)

$$\frac{M}{5.4 \text{ to } 6.6} \qquad \frac{R_N/R_B}{\approx 0.032}$$

Fig. 16 Variation of Zero-Lift Drag Coefficient with Reynolds Number (M $\approx$ 6)

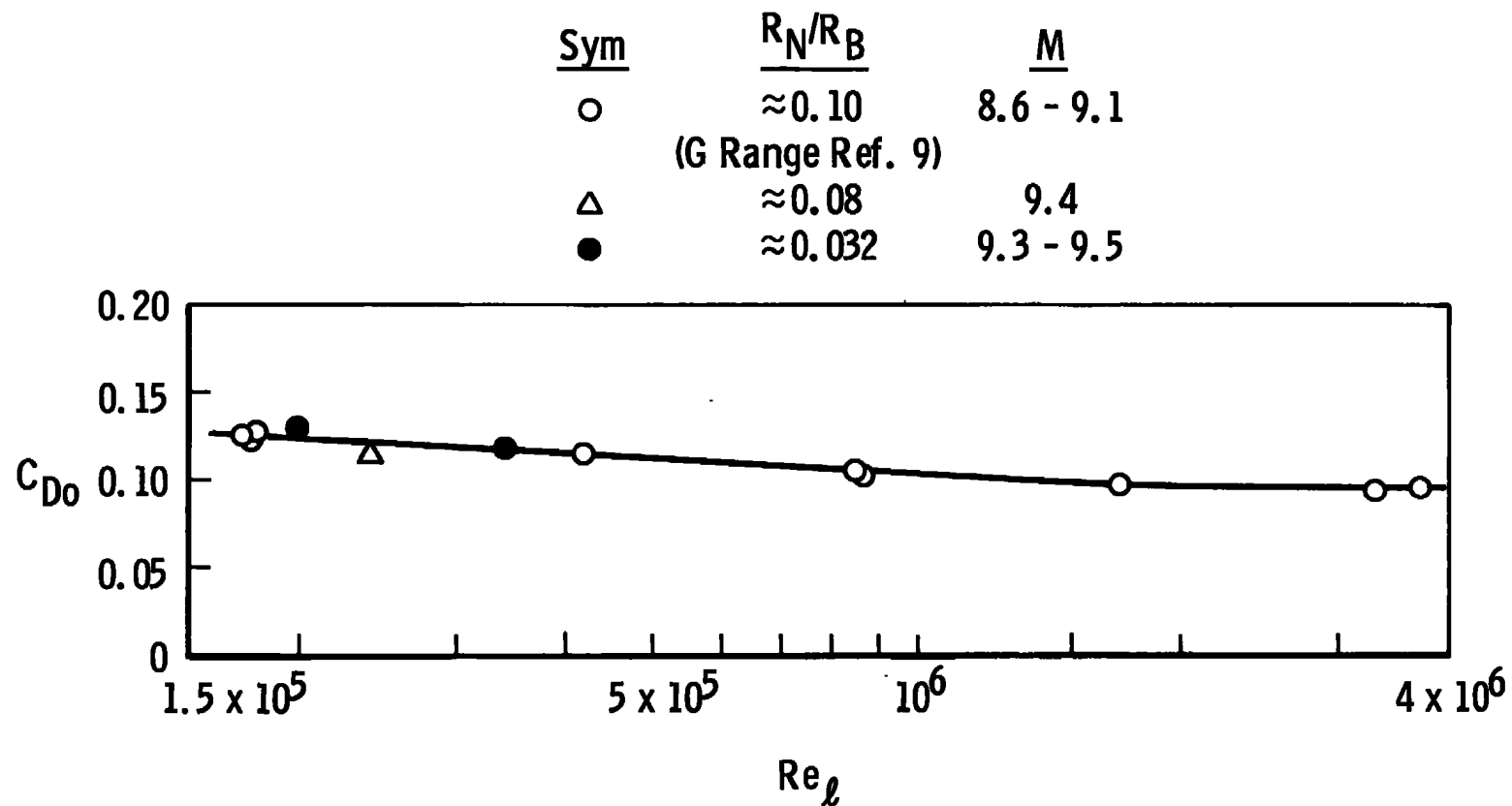| Sym	R_N/R_B	M
O	≈ 0.10	$8.6 - 9.1$
	(G Range Ref. 9)	
△	≈ 0.08	9.4
●	≈ 0.032	$9.3 - 9.5$

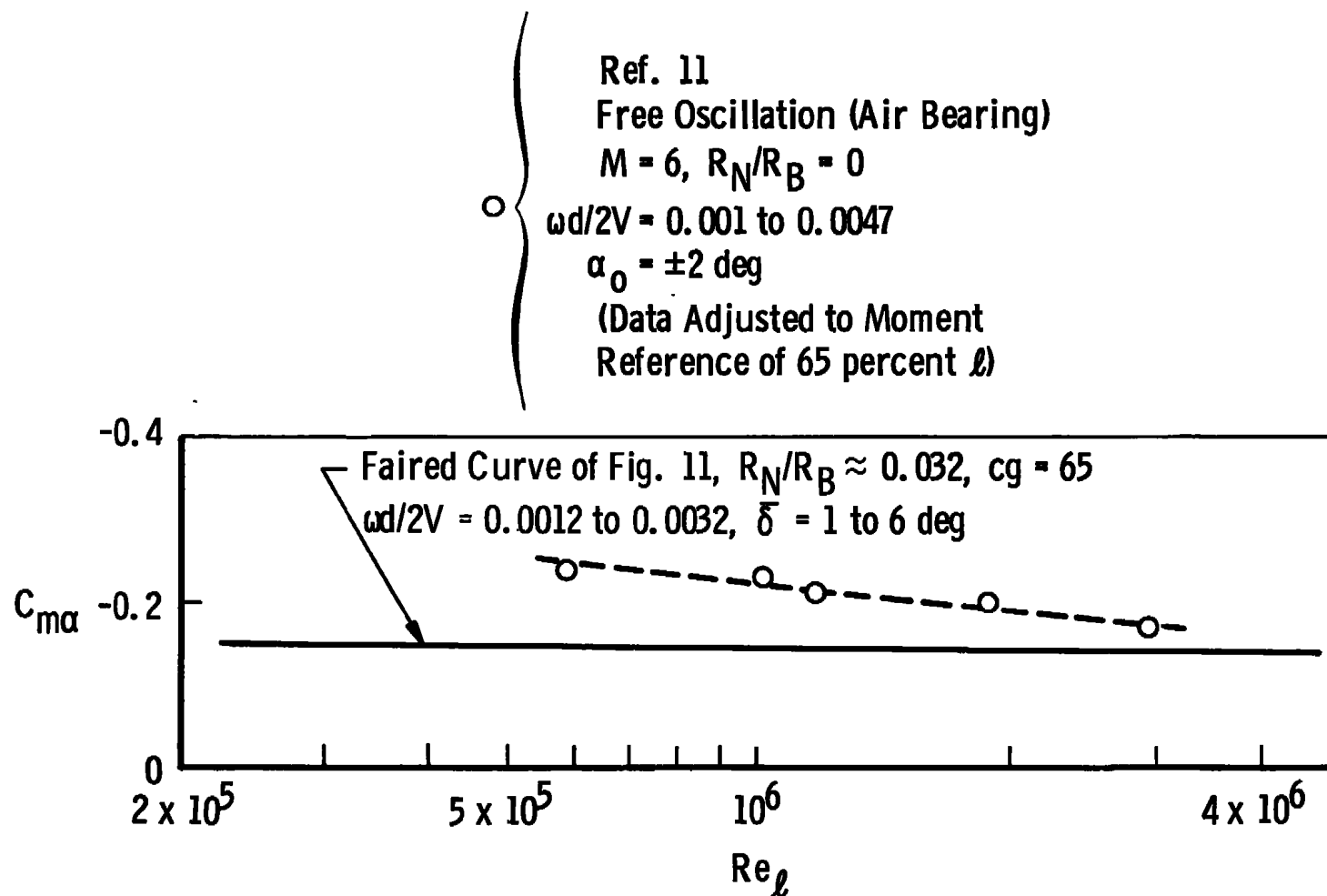Fig. 17 Variation of Zero-Lift Drag Coefficient with Reynolds Number (M $\approx$ 9)

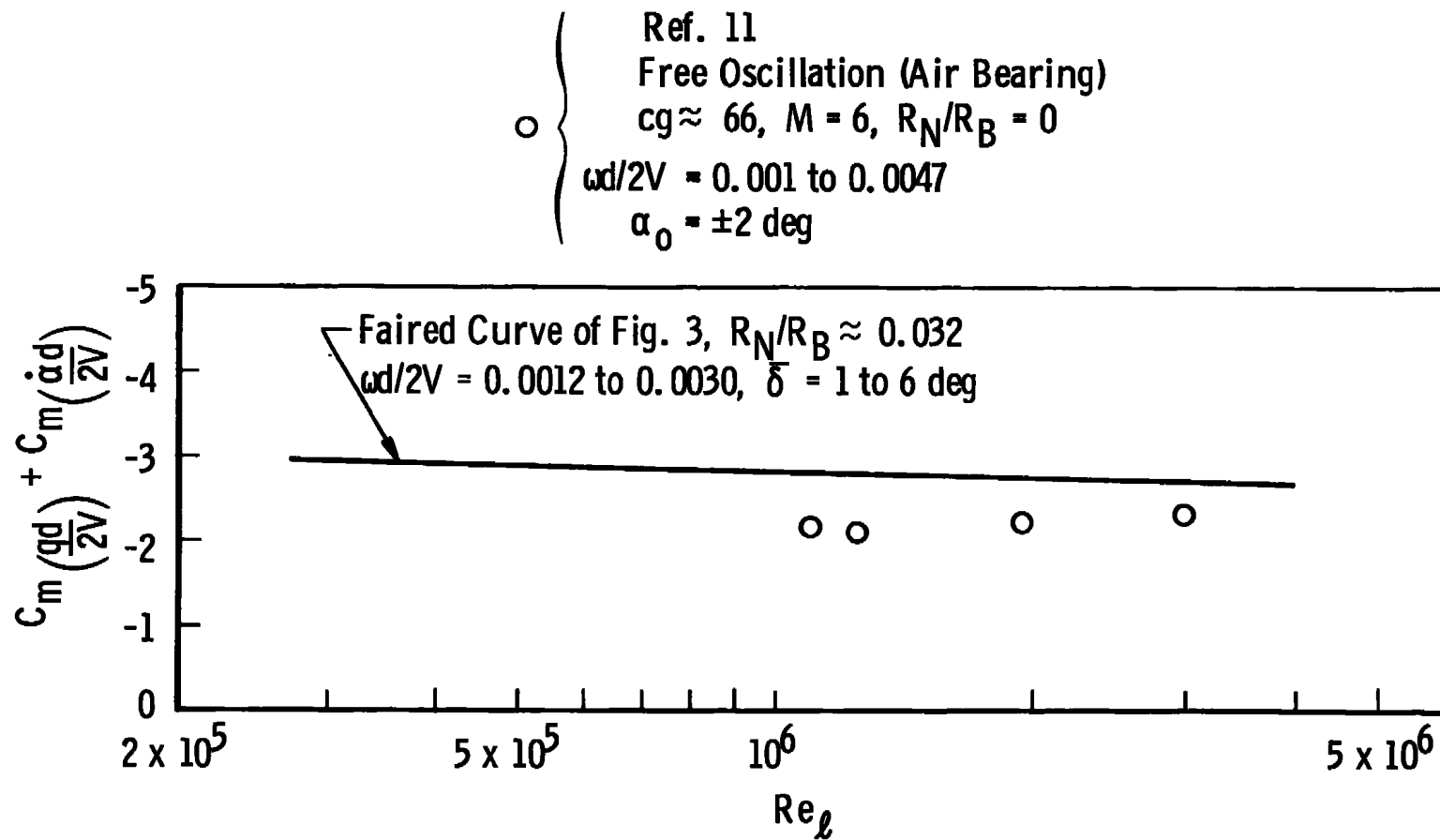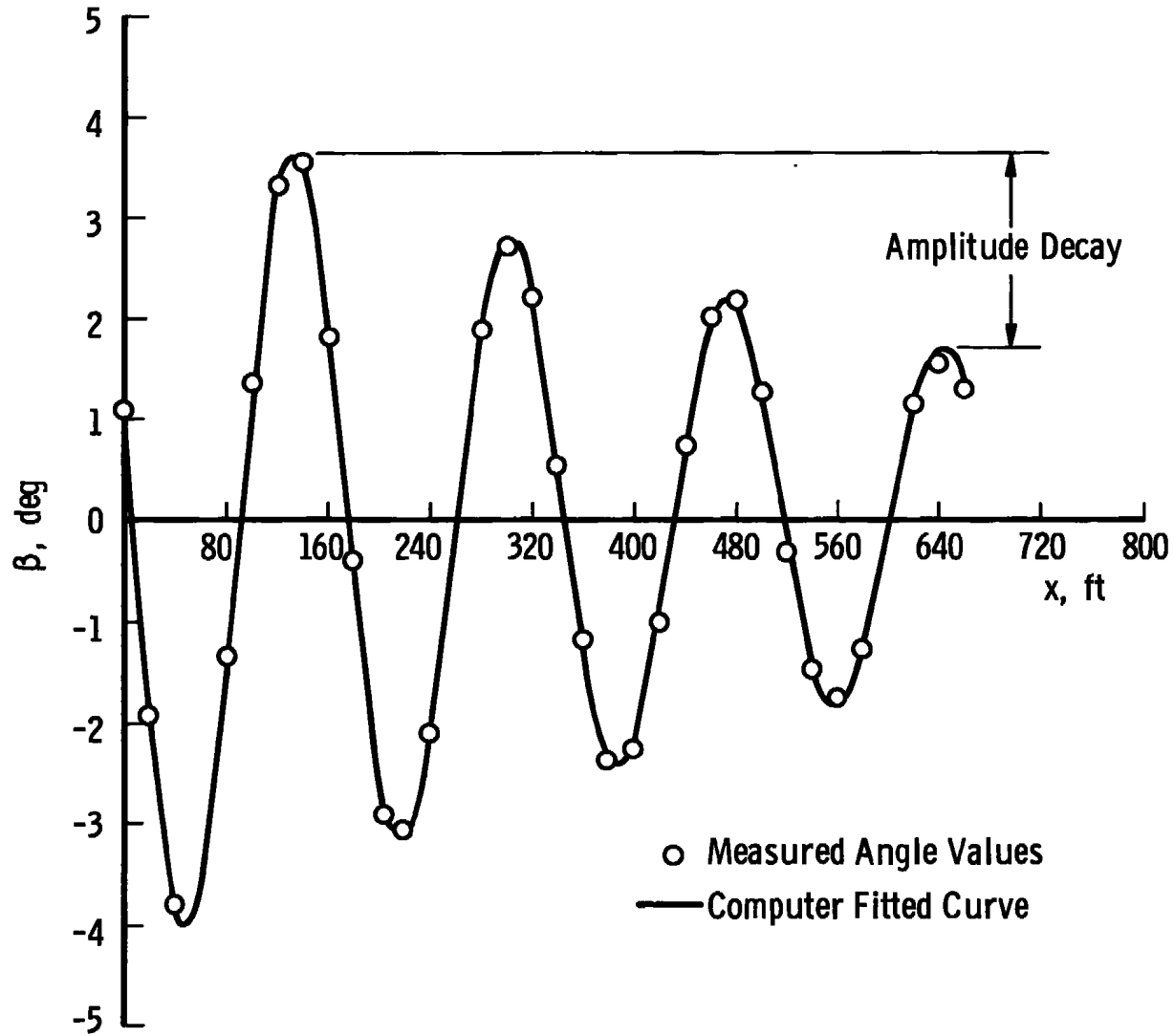Fig. 18 Comparison of Range and Tunnel $C_{m\alpha}$ Data at $M = 6$

Fig. 19 Comparison of Range and Tunnel Damping Data at M ≈ 6

Fig. 20 Motion Plot for Shot at $Re_\ell = 3.2 \times 10^6$

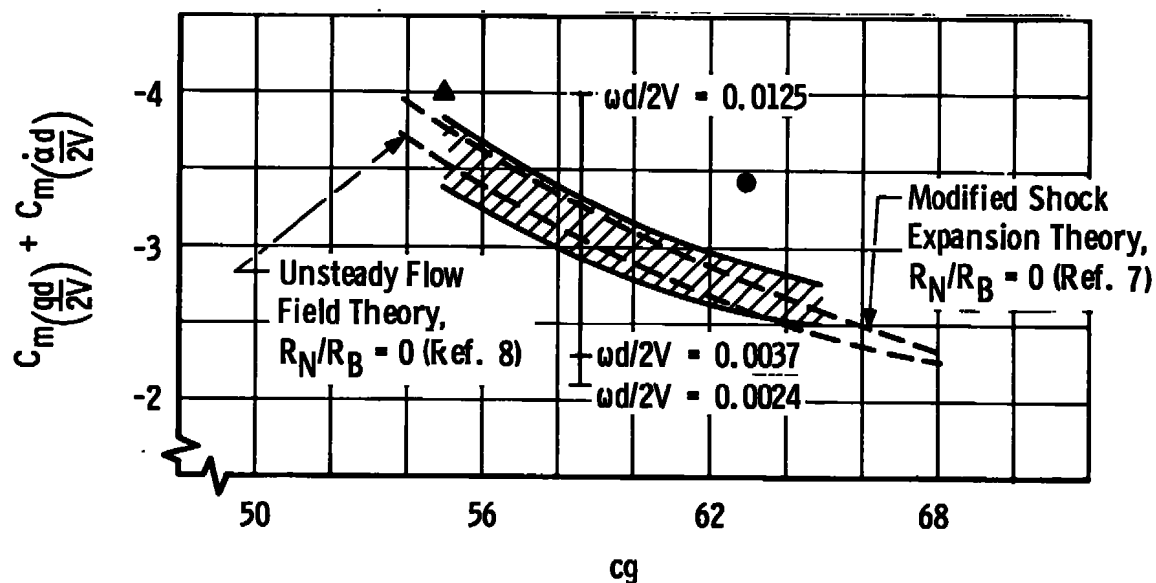| Sym	R_N/R_B	Re_ℓ	$\omega d/2V$	Amplitude, deg	Method Data Obtained	Facility (AEDC)
●	≈0.035	≈0.4 x 10^6	≈0.0012	$\bar{\delta} \approx 5$	Free-Flight Range	Range G
▲	0	≈10^6	0.003	$\bar{\delta} \approx 7$	Free-Flight Tunnel	Tunnel C
▨	0	≈10^6	0.002 to 0.004	α_0 = 2 to 8	Includes Both Free and Forced Oscillation, and Gas Bearing and Flexure Pivot Data	Tunnel C
I	0.017	0.36 x 10^6	0.0024 to 0.0125	α_{mean} = 1.5	Free Oscillation (Flexure Pivot) Ref. 12	Tunnel C

Fig. 21 Comparison of Range and Tunnel Damping Data at M ≈ 10

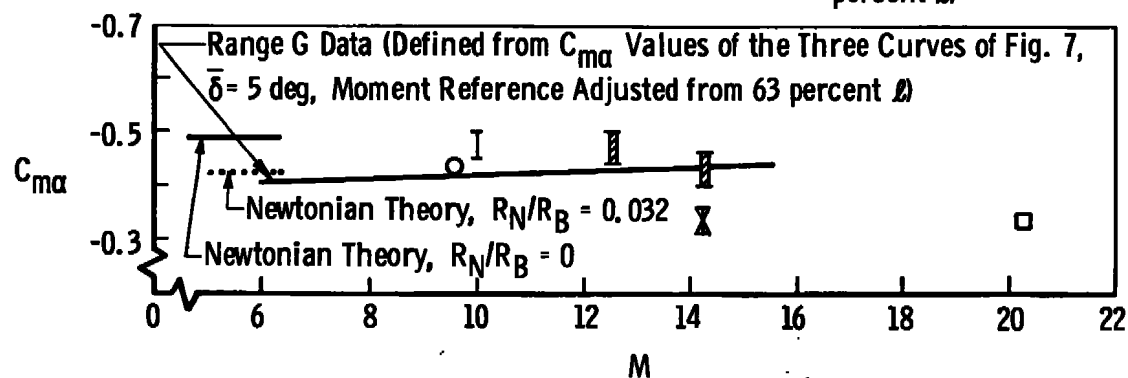| Sym	R_N/R_B	Re_l	$\omega d/2V$	Amplitude deg	Facility	Method Data Obtained
○	0.035	4.79×10^6	0.0024	$\bar{\delta} = 4.2$	VKF	Free-Flight (Moment Reference Adjusted from 65 percent l)
□	0	$\approx 0.165 \times 10^6$	0.0115	$\alpha_0 = 1.75$	LTV	Tunnel-Free Oscillation (Moment Reference Adjusted from 54.8 percent l)
⊥	0	0.45×10^6 to 0.50×10^6	0.0043	$\alpha_0 = 3$ to 8.5	VKF	Tunnel-Free Oscillation
▨	0.016	$\approx 0.65 \times 10^6$	0.0026 to 0.007	$\alpha_0 = 0.5$ to 5.5	ARL	Tunnel-Free Oscillation (Ref. 13)
⋈	0	$\approx 0.56 \times 10^6$	0.0147	$\alpha_0 = 1.75$	LTV	Tunnel-Free Oscillation (Moment Reference Adjusted from 54.8 percent l)

Fig. 22 Comparison of Range and Tunnel $C_{m\alpha}$ Data at High Mach Numbers (Moment Reference at 60 percent l)

Tunnel-Free Oscillation (Sting-Supported Models)

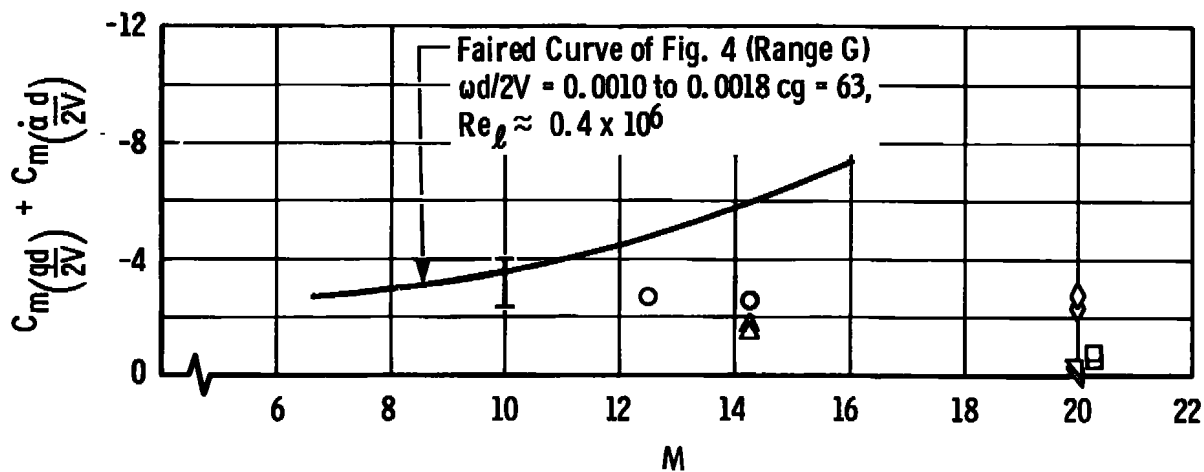| Sym	R_N/R_B	cg	Re_ℓ	$\omega d/2V$	Amplitude, deg	Facility	Ref. No.
O	0.016	60	$\approx 0.65 \times 10^6$	0.0026 to 0.007	$\alpha_0 = 0.5$ to 5.5	ARL	13
△	0	54.8	$\approx 0.56 \times 10^6$	0.0147	$\alpha_0 = 1.75$	LTV	
□	0	54.8	$\approx 0.165 \times 10^6$	0.0115	$\alpha_0 = 1.75$	LTV	
�X	0.017	58.7	0.35×10^6	0.0024 to 0.0125	$\alpha_{mean} = 1.5$	VKF	12
◊	0.0167	55	0.25×10^6	0.023	$\alpha_{mean} = 2$	VKF	12
▽	0.017	58.7	0.28×10^6	0.0019 to 0.0107	$\alpha_0 = 1.5$	ARL	14

Fig. 23 Comparison of Range and Tunnel Damping Data at High Mach Numbers

DOCUMENT CONTROL DATA - R & D

(Security classification of title, body of abstract and indexing annotation must be entered when the overall report is classified)

1 ORIGINATING ACTIVITY *(Corporate author)*	2a. REPORT SECURITY CLASSIFICATION
Arnold Engineering Development Center ARO, Inc., Operating Contractor Arnold Air Force Station, Tennessee	UNCLASSIFIED
	2b. GROUP N/A

3 REPORT TITLE

FREE-FLIGHT INVESTIGATION OF THE AERODYNAMIC CHARACTERISTICS OF A 10-DEG SEMIANGLE CONE AT MACH NUMBERS FROM 6 TO 16

4. DESCRIPTIVE NOTES *(Type of report and inclusive dates)*
May 1967 and June 1968 - Final Report

5. AUTHOR(S) *(First name, middle initial, last name)*

C. J. Welsh, G. L. Winchenbach, and A. N. Madagan, ARO, Inc.

6. REPORT DATE	7a. TOTAL NO. OF PAGES	7b. NO OF REFS
April 1969	50	15

8a. CONTRACT OR GRANT NO. F40600-69-C-0001	9a. ORIGINATOR'S REPORT NUMBER(S)
b. PROJECT NO. 8953	AEDC-TR-69-63
c. Program Element 62201F	9b. OTHER REPORT NO(S) *(Any other numbers that may be assigned this report)*
d. Task 03	N/A

10. DISTRIBUTION STATEMENT

This document has been approved for public release and sale; its distribution is unlimited.

11 SUPPLEMENTARY NOTES	12. SPONSORING MILITARY ACTIVITY
Available in DDC	Arnold Engineering Development Center, Air Force Systems Command, Arnold Air Force Station, Tennessee

13 ABSTRACT

A 1000-ft hypervelocity range was used to obtain the free-flight static and dynamic stability and drag data presented for a 10-deg semiangle cone. Measurements indicate that the damping-in-pitch derivatives for the cone increase appreciably with increasing Mach number between $M = 8$ and 16 at a Reynolds number (based on model length and free-stream conditions) of about 0.4×10^6. Further, $C_{m\alpha}$ for the cone decreases significantly as the nose-radius to base-radius ratio of the cone is increased up to 0.1 for amplitudes greater than about 5 deg. Comparisons of the range stability data with wind tunnel data (involving sting-supported models) obtained in different test facilities indicate that appreciable differences in $C_{m\alpha}$ and $(C_{mq} + C_{m\dot{\alpha}})$ exist in some cases.

DD FORM 1473 1 NOV 65

14. KEY WORDS	LINK A		LINK B		LINK C	
	ROLE	WT	ROLE	WT	ROLE	WT
aerodynamic characteristics						
hypervelocity wind tunnels						
dynamic stability						
static stability						
drag						
yaw						
conical bodies						
hypersonic wind tunnels						